State-of-the-Art of Polymer-Based Conductive Adhesives for Electromagnetic Protection Manufacturing

J.W. Yang, Y.S. Yang, H. Wu, S. Hussnain, X.J. Wang, H.B. Zeng* and W.J. Li*

MIIT Key Laboratory of Advanced Display Materials and Devices & Materials Physical and Chemical Research and Practice Center, College of Materials Science and Engineering, Nanjing University of Science and Technology, Nanjing 210094 P. R. China

Abstract: Polymer-based conductive adhesives (PbCAs) have emerged as key materials for electromagnetic wave interference (EMI) protection. They are increasingly replacing traditional metals due to their environmental friendliness, low-temperature processing, and flexibility. This review systematically elaborates on the conductive mechanisms of PbCAs, which are dominated by percolation theory and quantum tunneling effects. Furthermore, recent advances in the encapsulation of PbCAs within polymer matrices (*e.g.*, epoxy, polyurethane) and/or with conductive fillers (*e.g.*, metals, carbon-based materials, MXenes) have been highlighted. These innovations facilitate their expanded applications in EMI protection, including both EMI shielding and electromagnetic wave absorption. Despite significant advancements, challenges persist in balancing high conductivity with favorable mechanical properties and long-term stability under harsh service conditions. Future development is expected to focus on fillers with a low percolation threshold, optimized structural designs, and multifunctional applications in flexible and wearable electronics. These advancements aim to meet the requirements of miniaturized, high-performance electronic devices.

Keywords: Conductive polymers, Composite materials, Electromagnetic wave absorption, Electromagnetic interference shielding.

1. INTRODUCTION

With the evolution of electronic devices toward miniaturization and high power, electromagnetic radiation pollution has become a prominent challenge. This issue threatens device safety, the ecological environment, and human health [1-3]. Against this backdrop, developing material systems that integrate efficient electromagnetic shielding performance with good process adaptability is crucial [4-9]. Electrically conductive adhesives (ECAs) are composite materials that combine adhesion, electrical conductivity, and electromagnetic shielding functions. They are gradually replacing traditional metal shielding materials and tin-lead solders. This shift occurs because of their environmental friendliness, low processing temperatures, and compatibility with flexible substrates. They demonstrate broad prospects in fields such as electronic packaging, flexible electronics, and aerospace [10-14].

The core mechanism of electromagnetic shielding lies in attenuating energy through the reflection and absorption of incident electromagnetic waves[4–7,9]. Ideal shielding materials require strong absorption capacity, a broad operating frequency band, minimal thickness, and excellent flexibility. They also offer high dimensional and thermal stability, ease of processing, low cost, and long service life (Figure **1**). Although traditional metal materials exhibit significant shielding effectiveness, they are often heavy, prone to corrosion, and difficult to conform to complex structures. In contrast, ECAs adopt a composite design of an "insulating polymer matrix + conductive fillers," which maintains adhesive functionality while constructing conductive networks. This enables tunable shielding performance and better adaptation to the requirements of modern electronic devices for integration, lightweight design, and shape adaptability [12, 15-19].

The performance of ECAs primarily depends on the selection of matrix materials and conductive fillers, as well as the interactions between them [20]. Commonly used matrix materials include epoxy resin and polyacrylate resin. For example, epoxy-based ECAs are widely used in various packaging applications, such as chip mounting and circuit board interconnections. Their excellent adhesion, heat resistance, and chemical stability make them highly applicable for these uses [21, 22]. Polyacrylate-based ECAs, on the other hand, play a significant role in flexible displays and wearable devices because of their flexibility and light transmittance [23, 24]. Conductive fillers mainly include metal particles (*e.g.*, silver, copper), carbon materials (such as carbon nanotubes, graphene), and their composite systems. The morphology, content, and dispersion state of these fillers directly influence the formation of conductive pathways and shielding effectiveness [25-27].

In terms of conduction mechanisms, ECAs primarily rely on percolation effects and tunneling effects. When the filler concentration reaches the percolation

*Address correspondence to this author at the MIIT Key Laboratory of Advanced Display Materials and Devices & Materials Physical and Chemical Research and Practice Center, College of Materials Science and Engineering, Nanjing University of Science and Technology, Nanjing 210094 P. R. China; E-mail: wjli@njust.edu.cn; zeng.haibo@njust.edu.cn

Received on 24-11-2025 Accepted on 23-12-2025 Published on 30-12-2025

E-ISSN: 000-000/25

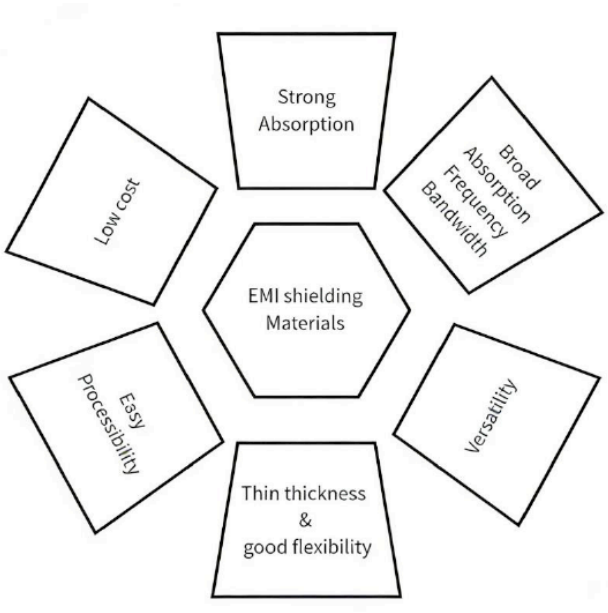

Figure 1: Desired properties of ideal EMI shielding materials.

threshold, a continuous conductive network forms between fillers. Electrons then achieve charge transport through direct contact or quantum tunneling. Shielding effectiveness arises from the reflection of electromagnetic waves on the material surface, multiple internal reflections, and absorption losses [28, 29]. By adjusting the filler type, morphology, orientation, and interface design, efficient electromagnetic shielding can be achieved at lower filler loadings. This technique helps maintain a balance between mechanical properties and process feasibility [20].

Despite their notable advantages, ECAs face multiple challenges in practical applications. High filler content can lead to a decline in mechanical strength. Besides, metal fillers may oxidize during long-term use, which causes a reduction in shielding performance. Moreover, humid-heat aging, thermal cycling, and other factors in complex environments can also affect their reliability [30-33].

In the future, with the rapid development of high-frequency and high-speed electronic devices, electromagnetic shielding materials will experience rapid progress. They will evolve toward high performance, multifunctionality, intelligence, and structure-function integration [34-37]. PbECAs possess strong design flexibility and good process compatibility. Therefore, they are expected to further expand their high-end applications in precision electronics and emerging flexible electronics through material innovation and structural optimization.

Currently, there is a lack of comprehensive and systematic reviews on the existing material systems for conductive adhesives. Based on this gap, the present article focuses on electromagnetic shielding conductive adhesives, providing a systematic review of research progress in their matrix materials and conductive fillers. It further outlines future development trends to offer meaningful insights for the design and application of high-performance electromagnetic-shielding conductive adhesives.

2. CONDUCTION MECHANISMS AND ELECTROMAGNETIC SHIELDING/ABSORPTION PRINCIPLES OF ELECTRICALLY CONDUCTIVE ADHESIVES

2.1. Conduction Mechanism of Electrically Conductive Adhesives

The fundamental principle of electrical conduction in PbCAs relies on the formation of a continuous conductive network by fillers within an insulating binder matrix. This network enables efficient charge transport. This process is governed by percolation theory and is significantly influenced by filler characteristics, interfacial interactions, and microstructure.

The most critical factor affecting the conductivity of PbCAs is the percolation threshold, which marks the pivotal transition point for conductive pathway formation. PbCAs typically composed of an insulating polymer matrix incorporating conductive fillers such as graphene, carbon black, carbon nanotubes (CNTs), or metal particles. Their electrical behavior depends strongly on the concentration of these fillers. At low filler volume fractions, particles are dispersed and isolated, resulting in conductivity similar to the insulating matrix. When the filler concentration reaches a critical value, known as the percolation threshold, a continuous conductive network spanning the entire

system is formed through direct contact or indirect interaction between filler particles. This network leads to a sharp increase in conductivity [12]. Beyond the percolation threshold, the conductive network further densifies, and the conductivity gradually stabilizes (Figure **2**). The value of the percolation threshold is significantly influenced by filler morphology, size, and distribution characteristics [13, 38]. Fillers with high aspect ratios (*e.g.*, graphene nanosheets, carbon nanotubes) can form conductive networks more readily due to their geometric advantages. This enhanced network-forming ability leads to substantially lower percolation thresholds. For example, the percolation threshold of graphene/polypropylene composites has been reported to be as low as 0.03 vol.% [39]. Whereas spherical fillers (*e.g.*, carbon black) require higher concentrations to form continuous pathways, their percolation threshold typically ranges from 3-30 vol.% [13]. Furthermore, the dispersion uniformity of the fillers also affects the percolation threshold. Moderate agglomeration can facilitate conductive network formation and lower the percolation threshold. Excessive agglomeration can conversely increase the percolation threshold and impair conductivity. For carbon-based materials, a microcapacitor effect is also observed. Conductive particles separated by the insulating matrix form numerous microcapacitor structures. These structures significantly enhance the dielectric properties, especially near the percolation threshold where the dielectric constant can increase by several orders of magnitude [12, 39 ,40].

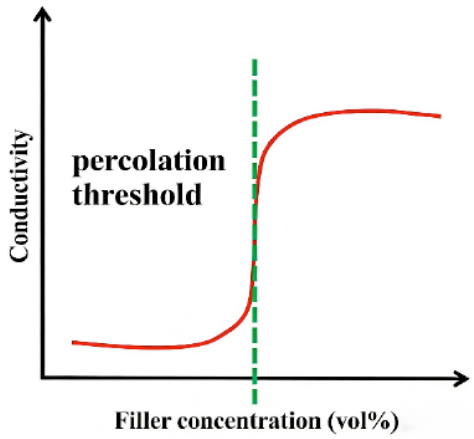

Figure 2: A typical percolation curve showing the abrupt increase in conductivity at the percolation threshold.

The charge transport mechanisms within the conductive network primarily include direct contact conduction and quantum tunneling conduction. These mechanisms determine the overall conductive efficiency of PbCAs [13, 18, 41]. Direct contact conduction is the most fundamental mechanism. When filler particles are in direct contact, electrons can flow freely through the conductive network formed by the fillers. The conduction efficiency then depends primarily on the intrinsic conductivity of the fillers themselves. Quantum tunneling conduction is an important supplementary mechanism when fillers are not in direct contact. Originating from quantum mechanical effects, electrons can tunnel through the thin insulating matrix barrier between fillers. This mechanism is highly sensitive to the inter-filler distance (d_c, typically 2-4 nm) and the barrier height of the matrix (λ). Smaller distances and lower barrier heights lead to higher tunneling efficiency [42].

Interfacial interactions are key factors influencing conductive efficiency. Oxide layers on metal fillers, surface functional groups on carbon materials, and the compatibility between intrinsically conductive polymers (ICPs) and the binder can all alter charge transport resistance. The use of coupling agents and surface modifications (*e.g.*, functionalization of carbon materials or coating of metal particles) can improve filler dispersion, enhance interfacial bonding, and reduce contact resistance. Synergistic effects between different fillers (*e.g.*, combining PANI with CNTs) can further lower the percolation threshold and enhance the stability and conductivity of the conductive network [41].

2.2. Composition and Classification of PbCAs

PbCAs generally consist of a non-conductive matrix to which conductive fillers are added. Standard PbCAs are only required to meet basic performance criteria for their designed application. In contrast, some specialized PbCAs additionally require properties such as high-temperature resistance, ultra-low temperature resistance, resistance to thermal cycling, and transparency. PbCAs can be classified into Anisotropic Conductive Adhesives (ACA) and Isotropic Conductive Adhesives (ICA). The difference between ACA and ICA lies in the filler loading level. For ICA, the conductive filler loading exceeds the percolation threshold, resulting in electrical conductivity in the X, Y, and Z directions. For ACA, on the other hand, the conductive filler loading is significantly below the percolation threshold. Electrical conductivity is provided only in the Z-direction after heat treatment and application of pressure [19, 43]. In recent years, Non-Conductive Adhesives (NCA) have also emerged. These adhesives do not require fillers but instead rely on relatively high bonding pressure combined with heat to achieve bonding [44, 45]. During the bonding process, heat and pressure are applied simultaneously for a period of time to allow direct physical contact between the two surfaces. A permanent connection is then formed upon curing of the NCA resin. Electrical conduction between the bottom and top contact pads is

achieved through contact via very fine, nano-scale rough concave-convex structures on the pad surfaces.

2.3. EMI Shielding Fundamentals

The purpose of electromagnetic shielding is to block or attenuate electromagnetic waves entering or leaving a specific area to prevent them from interfering with the normal operation of electronic equipment. The core of EMI shielding lies in the interaction between the material and the electromagnetic waves, weakening the intensity of the transmitted wave. Its mechanisms are primarily based on three distinct processes: reflection, absorption, and multiple reflections [46-48]. These mechanisms can be quantitatively evaluated using the Shielding Effectiveness (EMI Shielding Effectiveness, SE).

When electromagnetic waves impinge on the surface of a shielding material, reflection initially occurs due to the impedance mismatch between the material and free space, resulting in Reflection Loss (SE_R). This process originates from the interaction between charge carriers (electrons and holes) in the material and the electromagnetic field. Generally, the higher the electrical conductivity and the greater the abundance of charge carriers in the material, the more significant the reflection loss becomes. The electromagnetic waves that are not reflected enter the interior of the material, where their energy is attenuated through dielectric loss and magnetic loss, constituting the absorption loss (SE_A). Dielectric loss is related to the polarization characteristics of the material, including dipole orientation polarization and interfacial polarization. Magnetic loss stems from the magnetization and demagnetization processes of the material within an electromagnetic field. It involves mechanisms such as natural resonance, eddy current loss, and exchange resonance. When the electromagnetic waves that have penetrated the material reach the opposite surface, they are reflected again at the interface between the material and air. This phenomenon is known as multiple reflections. The corresponding loss is termed the Multiple Reflection Loss (SE_M) (Figure **3**). According to Schelkunoff's theory [49, 50], the total Shielding Effectiveness (SE_T) is the sum of these three components, as shown in Equation **1**.

$$SE(dB) = 10log_{10}\left(\frac{p_i}{p_t}\right) = SE_R + SE_A + SE_M \quad (1)$$

Here, p_i and p_t represent the power (or the intensity of the electric or magnetic field) of the incident and transmitted waves.

For the reflection loss, according to the definition of shielding effectiveness, it can be expressed as shown in Equation **2**.

$$SE_R = 20log_{10}\left|\frac{1}{T_{21}T_{12}}\right| \quad (2)$$

Here $\Gamma_1 = \frac{Z_2 - Z_1}{Z_1 + Z_2}$, $\Gamma_2 = -\Gamma_1$, $T_{21} = 1 + \Gamma_1$, $T_{12} = 1 + \Gamma_2$

Γ and T=1+Γ are the reflection coefficient and transmission coefficient, respectively, when the medium is of infinite thickness.

For the absorption loss, it is defined in Equation **3.**

$$SE_A = 20log_{10}|e^{yt}| \quad (3)$$

In this equation, t denotes the material thickness.

For the multiple reflection loss, the correction term is defined in Equation **4.**

$$SE_M = 20log_{10}\left|1 - \Gamma_1^2 e^{-2yt}\right| \quad (4)$$

The distance required for a wave to attenuate to 1/e of its original value is defined as the skin depth (δ). The multiple reflection effects can be neglected when the material thickness is greater than the skin depth or when the SE_A exceeds 10 dB. The quantitative calculation of EMI shielding effectiveness can also be

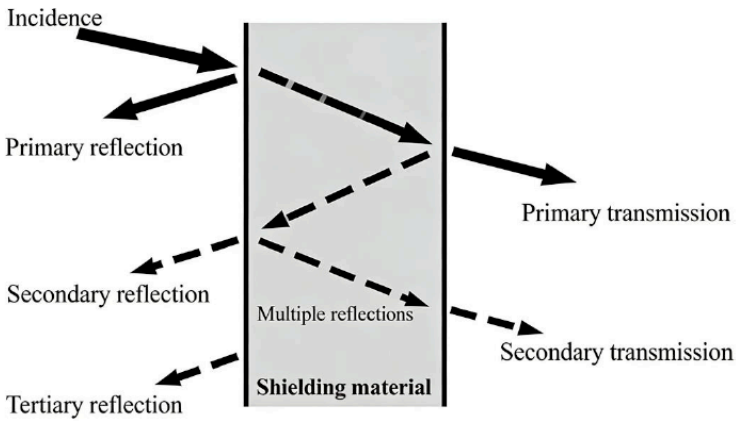

Figure 3: Schematic of propagation of the EM wave through a material sheet.

achieved through scattering parameters (S_{ij} parameters). These parameters can be measured using a vector network analyzer. By processing the electromagnetic measurement results with appropriate software, the electrical and magnetic properties can be inferred. S_{11} and S_{22} refer to the reflection coefficients measured at port 1 and port 2, respectively, while S_{12} and S_{21} represent the transmission coefficients [51]. For a single material, these parameters can be related to the reflectivity (R), transmittance (T), and absorptivity (A) through **Equations 5-7** [52].

$$R = |S_{11}|^2 = |S_{22}|^2 \quad (5)$$

$$T = |S_{12}|^2 = |S_{21}|^2 \quad (6)$$

$$A = 1 - R - T = 1 - |S_{11}|^2 - |S_{12}|^2 \quad (7)$$

The shielding effectiveness of a device can be evaluated through its S-parameters. The reflection loss and absorption loss can be calculated using Equations **8** and **9**.

$$SE_R = 10log_{10}|1 - |S_{11}|^2|\# \quad (8)$$

$$SE_A = 10log_{10}\left|1 - \frac{|S_{11}|^2}{|S_{21}|^2}\right|\#) \quad (9)$$

The EMI shielding performance is co-determined by both material properties and structural design. The material's electrical conductivity, magnetic permeability, and thickness directly govern the values of SE_R and SE_A. Structural features such as porous architectures and layered structures can prolong the propagation path of electromagnetic waves, enhancing multiple reflections and scattering. This interaction improves the shielding effectiveness [48, 53, 54]. Different types of materials exhibit distinct shielding mechanisms. Metal-based materials primarily rely on reflection, whereas carbon-based and MXene-based composites achieve highly efficient shielding through a synergistic combination of reflection and absorption. This provides diverse solutions for EMI protection.

2.4. Electromagnetic Wave Absorption Fundamentals

The fundamental principle of electromagnetic wave absorption lies in optimizing impedance matching to maximize the entry of electromagnetic waves into the material. Subsequently, the electromagnetic energy is dissipated by converting it into heat or other forms through mechanisms such as dielectric loss and magnetic loss. This process ultimately achieves efficient absorption. Its performance relies on the dynamic balance between impedance matching and energy attenuation capability [55-57].

Impedance matching is a prerequisite for effective electromagnetic wave absorption. The core requirement is that the material input impedance (Z_{in}) should approach the impedance of free space (Z_0, approximately 377 Ω) as closely as possible. Ideally, the impedance ratio Z_{in}/Z_0 should equal 1. However, due to the modulus value, situations may arise where Z_{in} and Z_0 differ significantly while the ratio still appears close to 1. Therefore, in practical evaluation, the delta function is employed to assess the impedance matching of the material [58, 59].

$$|\Delta| = |\sinh^2(Kfd) - M| \quad (10)$$

$$K = \frac{4\pi\sqrt{\mu'\varepsilon'}\sin\frac{\delta_\varepsilon+\delta_\mu}{2}}{c\cos\delta_\varepsilon\cos\delta_\mu} \quad (11)$$

$$M = \frac{4\varepsilon'\cos\delta_\varepsilon\mu'\cos\delta_\mu}{(\mu'\cos\delta_\varepsilon-\varepsilon'\cos\delta_\mu)^2+\left[\tan\left(\frac{\delta_\mu}{2}+\frac{\delta_\varepsilon}{2}\right)\right]^2(\mu'\cos\delta_\varepsilon+\varepsilon'\cos\delta_\mu)^2} \quad (12)$$

Ideal impedance matching is considered achieved when the calculated delta value is equal to or less than 0.4.

Attenuation capacity is another key factor determining electromagnetic wave absorption performance, and it can be characterized by the attenuation constant (α), which reflect the dissipation properties and overall attenuation capability of the material [60].

$$\alpha = \frac{\sqrt{2}\pi f}{c}\sqrt{(\mu''\varepsilon'' - \mu'\varepsilon') + \sqrt{(\mu''\varepsilon'' - \mu'\varepsilon')^2 + (\mu'\varepsilon'' + \mu''\varepsilon')^2}} \quad (13)$$

According to the equation 13, higher values of ε'' and μ'' lead to a larger attenuation constant, indicating that the material has stronger electromagnetic wave attenuation ability [61]. However, larger ε'' and μ'' values may also lead to impedance mismatch, potentially increasing reflection. It is thus essential to control the electromagnetic parameters within a reasonable range to balance impedance matching and loss capability.

The core of energy dissipation lies in the synergistic effect of dielectric loss and magnetic loss. Dielectric loss occurs through conduction loss and polarization loss. Conduction loss involves the formation of microcurrents by charge carriers under an alternating electric field, causing heat dissipation due to resistance. Its strength is positively correlated with electrical conductivity. However, the conductivity needs to be maintained within a moderate range to avoid excessively high values that could disrupt impedance matching [62]. Polarization loss in the GHz frequency band primarily involves dipole polarization and interfacial polarization. Dipole polarization refers to the delayed rearrangement of polar molecules or defect

sites in response to an electric field. While interfacial polarization arises from charge accumulation at heterogeneous interfaces, it is commonly observed in composite materials [63, 64]. Magnetic loss dissipates the magnetic field component and is primarily associated with magnetic materials. It includes eddy current effects, hysteresis loss, and resonance loss. Resonance loss includes natural resonance and exchange resonance. Natural resonance is mainly influenced by the anisotropy coefficient and saturation magnetization [65], whereas the frequency of exchange resonance is much lower than that of natural resonance [66]. Eddy current loss involves heat generation through closed currents induced by an alternating magnetic field. Excessive loss must be suppressed through methods such as nanonization and insulation coating to avoid disrupting impedance matching. Hysteresis loss and domain wall resonance typically occur only in weak electromagnetic fields and the MHz frequency range [67].

Porous, layered, or core-shell structures within the material can induce multiple reflections and scattering of electromagnetic waves. These effects prolong the propagation path and increase the probability of energy dissipation [57]. For instance, the 3D porous structure of MXene aerogels forms a continuous network of pores that forces electromagnetic waves to undergo multiple reflections and scattering within the channels. This significantly extends the propagation path and enhances the probability of energy dissipation [68]. Synergistic effects such as dielectric-magnetic synergy and heterogeneous interface synergy, can simultaneously optimize impedance matching and attenuation capacity [56, 69]. These mechanisms serve as key design principles for high-performance electromagnetic wave absorbing materials.

3. COMMON POLYMER MATRICES IN ECAS

Polymer resins are the most widely used matrix materials for adhesives, and they are primarily categorized into thermoplastic and thermosetting types. Thermoplastic resins (*e.g.*, polyethylene, polyamide) can be repeatedly softened by heating and hardened upon cooling. Thermosetting resins (*e.g.*, epoxy, polyurethane) form a three-dimensional network structure through cross-linking reactions and exhibit excellent dimensional stability and heat resistance [70, 71]. These materials play crucial roles in fields such as aerospace, electronic packaging, and biomedical applications. They are currently undergoing rapid development toward intelligentization (self-healing, shape memory), greening (bio-based monomers,

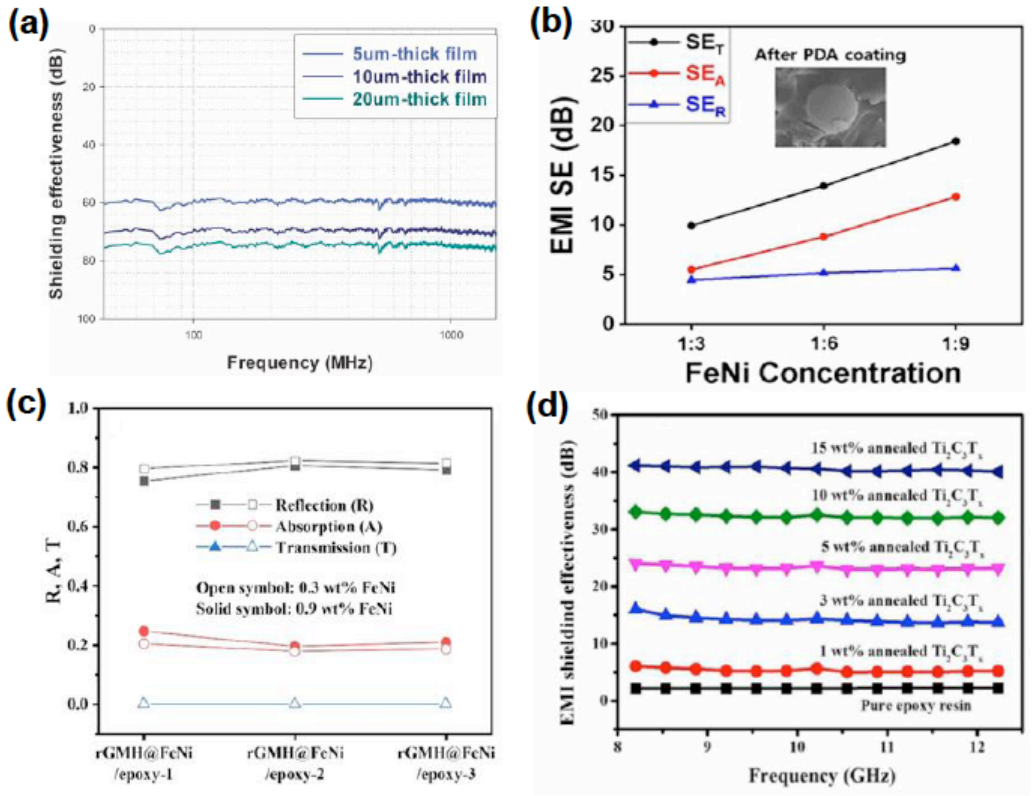

Figure 4: (**a**) SE data plot of various conductive films in the range of 30MHz ~ 1.5GHz. Reproduce with permission [91] Copyright, 2018 Elsevier. (**b**) EMI shielding performance by different FeNi concentrations after PDA surface coating. Reproduce with permission [92] Copyright, 2024 Wiley-VCH Verlag GmbH. (**c**) R, A and T coefficients of rGMH@FeNi/epoxy EMI shielding composites with different f-FeNi loading methods. Reproduce with permission [93] Copyright, 2025 Elsevier. (**d**) Annealed $Ti_3C_2T_x$/epoxy EMI shielding nanocomposites. Reproduce with permission [94] Copyright, 2019 Elsevier.

degradable designs), and high performance (nanocomposites, multifunctional integration) [72-77]. They have become a vital foundation for promoting technological innovation and sustainable development in modern industry.

3.1. Epoxy Resin

Epoxy resin was first discovered by Prilezhaev in 1909 [78]. It is defined as a low molecular weight prepolymer containing at least one epoxy group. As a thermosetting resin, epoxy can be cured using various hardeners via cross-linking reactions. Its final properties depend on the specific combination of the epoxy resin type and the hardener system [79-84]. They demonstrate outstanding mechanical properties, high adhesion to various substrates, and excellent chemical corrosion and heat resistance. Owing to these advantages, they are extensively used in fiber-reinforced composites, general-purpose adhesives, high-performance coatings, and encapsulating materials [85-90].

Ag/Epoxy Resin Composites were prepared for electromagnetic shielding in high-frequency FCBGA packages [91]. Studies show that flake-shaped silver particles can form an effective surface-contact network, significantly reducing contact resistance. At a silver content of 90–92 wt.%, the composite achieves a minimum resistivity of 2.9×10^{-7} Ω·m(Figure **4a**). Using an air spray process, the material with thicknesses of 5 μm, 10 μm, and 20 μm exhibits shielding effectiveness (SE) of 60 dB, 65 dB, and 70 dB, respectively, in the frequency range of 30 MHz – 1.5 GHz. Although this study did not directly quantify the contributions of absorption and reflection, the high conductivity and SE values indicate that the composite functions as a typical reflection-dominant shielding material within this frequency band.

Polydopamine-Coated FeNi/Epoxy Composites were developed to address key challenges in polymer-based EMI shielding, specifically filler sedimentation and poor interfacial adhesion [92]. The surface modification with PDA created chemical bonds between the FeNi filler and the epoxy matrix, which fundamentally improved filler dispersion and interfacial bonding—critical structural factors determining performance. increasing the FeNi content from 75 wt% to 90 wt% enhanced the total shielding effectiveness (SE□) at 12 GHz from 9.12 dB to 17.86 dB (Figure **4b**). The SE was deconvoluted, revealing that absorption loss (SE_a) constituted the dominant contribution, increasing from 5.15 dB to 12.28 dB, while reflection loss (SE_r) saw a comparatively modest rise. This absorption-dominant behavior is attributed to the high magnetic permeability of the FeNi alloy, which promotes magnetic loss and eddy current dissipation within the composite, distinguishing it from conductive-filler-dominated reflective shields. Concurrently, the thermal conductivity increased significantly from 0.63 $W \cdot m^{-1} \cdot K^{-1}$ to 1.49 $W \cdot m^{-1} \cdot K^{-1}$, and the composite exhibited excellent thermal stability with a residual mass of approximately 89% at 700°C.The PDA coating dramatically enhanced mechanical robustness, with the nanoindentation elastic modulus increasing by an order of magnitude to 1.29 GPa and hardness rising substantially, underscoring the critical role of interfacial engineering in achieving multifunctional performance.

rGMH@FeNi/Epoxy Composites were prepared to reduce the reflection of traditional shielding materials by constructing a "reduced graphene oxide-MXene-FeNi" honeycomb structure [93]. With only 5.4 wt% filler content (including 0.9 wt.% FeNi), the composite achieved a shielding effectiveness in the X-band reached 61 dB (Figure **4c**), with a reflection loss of only 6 dB and an absorption rate of 90.2%. This outstanding "high absorption, low reflection" characteristic stems from its structural design: the introduction of the honeycomb skeleton and magnetic FeNi particles effectively improves the impedance matching at the material's surface, allowing more electromagnetic waves to penetrate the interior. Subsequently, the waves undergo multiple reflections and scattering within the continuous conductive-magnetic 3D network and are efficiently dissipated through various mechanisms such as ohmic loss from the conductive network, hysteresis loss from FeNi, and polarization loss at heterogeneous interfaces. Furthermore, The material exhibited good thermal stability, and its storage modulus increased by 48.4% compared to pure epoxy.

The Annealed $Ti_3C_2T_x$ MXene/Epoxy Nanocomposite was successfully fabricated for high-performance electromagnetic interference shielding [94]. In this study, Annealing effectively removed partial polar functional groups (*e.g.*, -F, -OH) from the MXene surface, reducing electron transport resistance and thereby significantly enhancing the intrinsic conductivity and shielding effectiveness of the composites. At a filler content of 15 wt%, this material exhibits an outstanding electrical conductivity of 105 S/m and the total shielding effectiveness reached 41 dB in the frequency range of 8.2–12.4 GHz. They represent improvements of 176% and 37%, respectively, compared to its non-annealed counterpart. Furthermore, with a 5 wt% filler content, it demonstrates optimal mechanical properties, including a Young's modulus of 4.32 GPa and a hardness of 0.29 GPa. This work demonstrates that medium-low

Table 1: Properties of Representative Materials

System	Filler Type & Content	Thickness	Shielding Effectiveness (SE_t) / Frequency Band	Mechanical Properties & Flexibility
Ag/Epoxy [91]	Flake-shaped Ag (90-92 wt%)	5-20 μm	60-70 dB(for 5-20 μm) 30 MHz – 1.5 GHz	not specified
PDA@FeNi/Epoxy [92]	FeNi alloy (75-90 wt%)	0.7 mm	9.12 – 17.86 dB @ 12 GHz	Elastic modulus up to 1.29 Gpa (after PDA coating)Rigid material
XSBL/SA/CNTs emulsion-based adhesive[95]	CNTs, 15 wt%	Three-layer plywood (thickness not specified)	32 dB (X-band, 8.2–12.4 GHz)	Dry bonding strength: 4.48 MPa; room-temperature curable, flexible
SiO_2@Ag@MF superhydrophobic porous foam[96]	Ag coating (thickness varied), MF foam matrix	2 mm	65 dB (X-band, 8.2–12.4 GHz)	Flexible, bendable, corrosion-resistant, lightweight (density: 0.014–0.019 g/cm³)
PS/EMA/FCNT or FCNF thermoplastic elastomeric blend composites[97]	FCNT or FCNF, 15 wt%	~1 mm	34.9 dB (FCNT), 36.7 dB (FCNF) (X-band, 8.2–12.4 GHz)	Thermoplastic elastomer system, offers flexibility and mechanical strength
Ag-decorated PVA/Fe_2O_3 nanofibrous composites[98]	Ag coating (200 nm), Fe_2O_3 nanoparticles (10 wt%)	Nanofibrous mat (overall thickness not specified)	45.2 dB (at 10 GHz, measured from 0.5–18 GHz)	Nanofibrous structure, lightweight, flexible, porous, absorption-dominant
Acrylate pressure-sensitive adhesive (a-PSA) composite[99]	Nickel chains (Ni chains) in acrylate PSA; 30.0 wt% Ni chains	0.18 mm	36.31–39.97 dB in X-band (8.2–12.4 GHz)	Peel strength: 39.56 N/m; shear strength: 41.07 kPa; static shear adhesion: 612.87 min; highly flexible and can be rolled/twisted
Silicone rubber (SR) sandwich composite[100]	Carbon fiber @ Fe_2O_3 (CF@Fe_2O_3) as middle layer; BN/SR as outer layers; 45.5 wt% CF@Fe_2O_3 + 20.6 wt% BN	~740 μm	37.7 dB in X-band (8.2–12.4 GHz)	Flexible and bendable; volume resistivity: 6.2×10^{14} Ω·cm; breakdown strength: 26.8 kV/mm; used as thermal interface material

temperature annealing is an effective and environmentally friendly (compared to chemical reduction) surface engineering strategy that can significantly enhance the overall shielding performance of polymer-based composites by optimizing the electrical properties of the filler.

3.2. Polyurethane-Based PbCAs

Polyurethane is a high-strength polymer whose material properties are predictable and scalable, and it can be used compositely with most substrates. Polyurethane has diverse application forms, with the most common products including rigid/flexible foams, coatings, cast elastomers, fibers and fabrics, adhesives, sealants, thermoplastics, compounded rubbers, and composite systems [21, 22, 101]. As an adhesive, its characteristics such as self-supporting nature, excellent bonding strength, rapid curing, and weather resistance give it a leading position among numerous polymer materials [102-104].

TA-Modified MXene/Waterborne Polyurethane Composite Coating was developed as an eco-friendly coating that integrates absorption-enhanced EMI shielding and infrared (IR) stealth functions to reduce electromagnetic wave secondary pollution [105]. The coating achieves a shielding effectiveness of 37.4 dB in the X-band (8.2–12.4 GHz) (Figure **5a**) with an absorption coefficient of 0.41. This superior performance originates from the spontaneously formed gradient distribution architecture of fillers (Figure **4**). driven by gravity after TA-induced MXene sheet agglomeration and weakened MXene-WPU interaction. A significant conductivity gradient increasing from the top (WPU-rich region) to the bottom (MT-rich region) is established (Figure **5j**). which effectively optimizes the surface impedance matching, allowing more electromagnetic waves to penetrate and thereby enhancing the shielding performance. After 72 hours of exposure to various harsh conditions, its shielding effectiveness retention rate remains above 93%. It achieves an adhesion rating of 0 on an aluminum alloy substrate and withstands ultrasonic treatment, and possesses a minimum pull-off adhesion strength of 2.58 MPa

Diels-Alder Bond Cross-Linked PU/CNT Self-Healing Composite was developed to address the inevitable damage to electromagnetic interference shielding materials during long-term use and to achieve

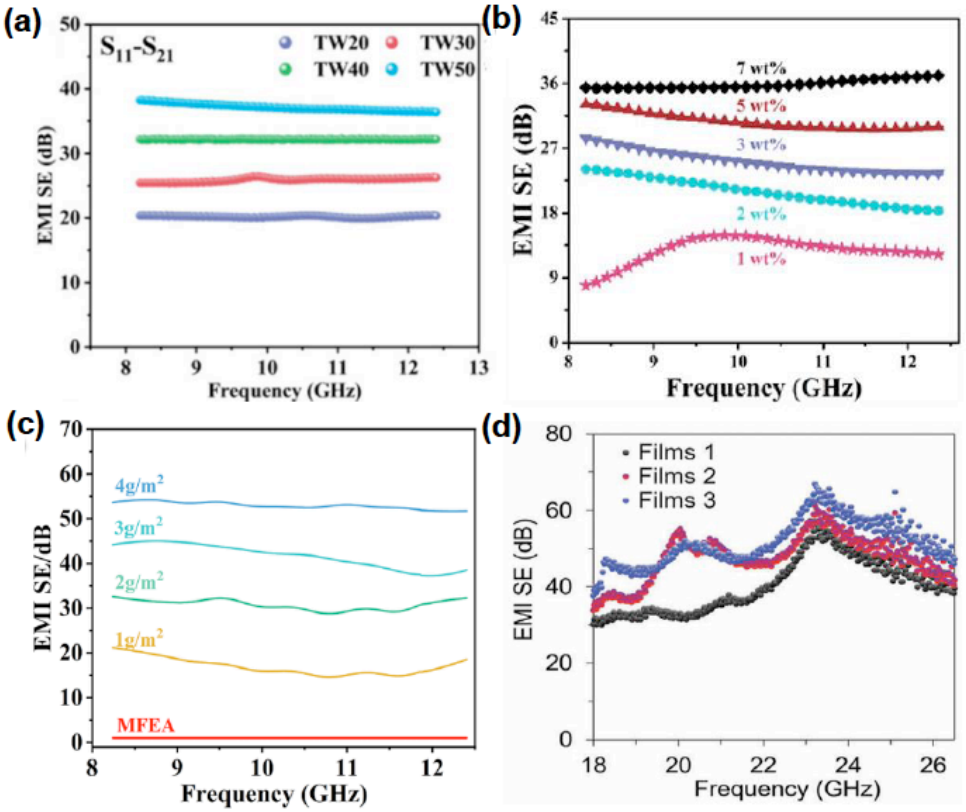

Figure 5: (**a**) EMI shielding property of TW coatings calculated. Reproduce with permission [105] Copyright, 2025 Elsevier. (**b**) EMI SE as a function of frequency in X-band frequency range for the PUDA/CNT composites. Reproduce with permission [106] Copyright, 2020 Elsevier. (**c**) Electromagnetic shielding efficiency at different AgNWs concentrations. Reproduce with permission [107] Copyright, 2023 Elsevier. (**d**) EMI shielding effectiveness (SE) values for stacked PEDOT-rich nanofibril films with total thickness of ≈25, 50, and 75 μm. Reproduce with permission [108] Copyright, 2024 Wiley-VCH Verlag GmbH.

reliable EMI shielding [106]. With a CNT content of 5 wt%, the material exhibits an EMI SE of 30.7 dB in the X-band (8.2–12.4 GHz) (Figure **5b**), with absorption loss contributing 90.9%, This is primarily attributed to the well-established three-dimensional conductive network formed by the homogeneous dispersion of CNTs within the polymer matrix (Figure **2**). This network enhances the overall electrical conductivity, leading to efficient Ohmic loss that converts incident electromagnetic wave energy into heat. With the increase in CNT loading, the tensile strength and Young's modulus of the material significantly improve, while the elongation at break (EB) decreases correspondingly. For PUDA/CNT–7 wt%, the tensile strength reaches 24.0 ± 0.7 MPa, representing a 105% increase compared to pure PUDA (11.7 ± 1.2 MPa), while maintaining a relatively high elongation at break of 342% ± 10%.

Oxime-Urea Bond Polyurethane/AgNWs Multifunctional Composite was developed for stretchable, self-healing, and recyclable EMI shielding, while also integrating Joule heating and human motion monitoring functions [107]. At an AgNWs areal density of 4 g/m², it achieves a maximum shielding effectiveness of 53.6 dB in the X-band, (Figure **5c**) and remains >35 dB under 30% strain. It integrates Joule heating (reaching 53°C within 15 s under 1.5 V) with highly sensitive strain sensing (gauge factor up to 28.35). The single lap-shear strength on stainless steel is 1430 kPa, and it maintains stable adhesion even at -27°C.

The PEDOT: PSS/Supramolecular Polyurethane Blend Multilayer Film was developed for absorption-dominated EMI shielding and microwave absorption (MWA) in flexible electronics [108]. The film achieves an exceptionally high thickness-normalized SE of 175 dB/mm in the K-band (18–26.5 GHz) (Figure **5d**), with an absorption bandwidth of 8.5 GHz. Under 150% uniaxial stretching, its SE remains at 122 dB/mm. The outstanding performance originates from its unique structural design: the anisotropic conductive network formed by microphase separation and the insulating elastomer phase induce significant interfacial polarization, while the multiple reflections of electromagnetic waves at the multilayer interfaces greatly prolong the propagation path, thereby effectively converting energy into heat. It can self-heal cutting damage within 60 seconds at room temperature (98% SE recovery rate). With cell viability >95%, Regarding environmental and sustainability aspects. While the supramolecular design endows the film with

excellent self-healing ability—extending service life and reducing waste—the long-term environmental fate of its components (PEDOT:PSS, boron oxide nanoparticles) requires further study. The blend presents challenges for conventional polymer recycling streams due to its multi-component, intimately mixed nature. Although biocompatible, a full lifecycle assessment considering raw material sourcing, manufacturing, and end-of-life disposal or degradation is necessary to evaluate its overall environmental footprint compared to traditional shielding materials.

3.3. Acrylate-Based PbCAs

Polyacrylates (such as polymethyl acrylate, polyethyl acrylate, polybutyl acrylate, etc.) are polymerization products of acrylate monomers [109], commonly used as adhesives, coatings, films, and textiles [110-112]. Their advantages include removable characteristics (degradable under specific conditions [113, 114]), low density, high transparency, good film-forming ability, moderate aging resistance, low environmental pollution, and excellent adhesive. These properties fully meet the requirements of modern bonding applications. A notable characteristic is its piezoresistive effect [115], which enables light pressure to generate rapid and tight adhesion of bonded objects, aligning with the demands of efficient operation.

Nickel Chain/Acrylic Pressure-Sensitive Adhesive Composite was developed to protect portable electronic products and wearable devices from unwanted microwave radiation and to achieve tunable EMI shielding [116]. With a thickness of 0.18 mm and 30.0 wt% filler, the material achieves an SE of 39.97 dB in the X-band, 71% of which is attributed to absorption loss. This efficient microwave attenuation stems from the synergy of multiple loss mechanisms:the continuous nickel chain network provides significant conduction loss; the abundant interfaces between the nickel chains and the insulating polymer matrix induce strong interfacial polarization relaxation; the intrinsic magnetism of nickel contributes to magnetic losses ;and the distinctive gradient layered structure promotes multiple internal reflections and scattering of electromagnetic waves, substantially prolonging the attenuation path and converting energy into heat. It also exhibits excellent adhesion (peel strength: 39.56 N/m; shear strength: 41.07 kPa), adheres to various substrates, and causes no skin irritation.

A Highly Adhesive Nickel Powder/Acrylic Copolymer Conductive Adhesive Film was developed for electromagnetic wave shielding in flexible electronic products and other scenarios, combining strong adhesion with excellent shielding performance [117]. By optimizing the acrylic acid content and introducing a cross-linked structure, the material achieves a synergy of high adhesion and high shielding, As the acrylic acid content increased from 2% to 8%, the adhesion strength rose from 504.73 N/m to 812.6 N/m, with a peel strength of 700.79 N/m that retains 95.84% after aging at 85°C/85% RH for 48 hours. At a nickel powder content of 20 wt.% its average SE across the broad 9 kHz–8.5 GHz frequency band is 63.7 dB, along with extremely low contact resistance (horizontal: 0.11 Ω; vertical: 0.43 mΩ). The shielding mechanism is reflection-dominant: the underlying nickel/copper composite conductive fabric serves as the primary high-reflection barrier, while the uniformly dispersed nickel network within the acrylic adhesive layer further dissipates electromagnetic energy through synergistic conduction loss (ohmic loss) and internal multiple reflections. From an industrial perspective, the fabrication process involving solution casting, drying (120°C for 3 min), and laminating is scalable. The material demonstrates promising reliability, with the optimized formulation (D-LAT_CL 03 + 20 wt% Ni) retaining 95.84% of its initial peel strength (700.79 N/m) after an accelerated aging test at 85°C/85% RH for 48 hours, indicating robust long-term stability under harsh conditions. Regarding environmental and sustainability aspects, while the acrylic matrix and Ni are not inherently biodegradable, the use of Ni powder—a commercially viable and relatively low-toxicity metal compared to alternatives like lead—presents a pragmatic choice. However, end-of-life recyclability remains a challenge due to the strong adhesive bonding and composite nature, necessitating future research into disassembly or chemical separation processes to improve lifecycle management.

3.4. Polyimide-Based PbCAs

Polyimides represent a highly promising class of engineering polymers due to their exceptional thermal stability, cryogenic performance, and mechanical strength. They also offer excellent resistance to chemical corrosion and radiation, flexibility, and outstanding dielectric properties. Their outstanding performance and unparalleled versatility make them unique among numerous polymer materials. Polyimides encompass both thermosetting and thermoplastic categories and can be synthesized via polycondensation or addition mechanisms. Due to the vast variety of their monomer precursors, the structure-property relationships are often difficult to predict fully, thus fostering an extremely wide range of application fields [118-121]. Since their first successful synthesis by DuPont chemists in the 1950s. This material has evolved into a true high-performance

engineering material, particularly in high-end manufacturing sectors like microelectronics and aerospace.

Anisotropic MXene@PI Hybrid Foam was prepared to explore the effect of direction-dependent pore structure [122]. Cross-linking via copper ion-π interactions and enhanced interfacial bonding result in a direction-dependent pore structure. When five layers of MXene nanosheets were incorporated, the anisotropic MXene@PI-5 hybrid foam demonstrated an exceptional EMI SE of 62.7 dB. The shielding mechanism evolves with the number of MXene coatings: when the coating layer is ≤1, absorption slightly outweighs reflection; when the coating layers are ≥2, the material's conductivity increases substantially, leading to greater impedance mismatch with air and shifting the dominant mechanism to reflection-dominated (the reflection coefficient R significantly surpasses the absorption coefficient A). The tubular structure in the vertical direction is more effective in trapping and attenuating electromagnetic waves, which is the key physical reason for its superior performance over the honeycomb structure in the parallel direction. The introduction of cation-π interactions for cross-linking enhanced the mechanical properties of the polyimide foam. The foam with a 30% molar ratio of Cu^{2+} achieved a yield strength of 2.4 MPa, which is significantly higher than the 0.45 MPa of the pure polyimide foam.

Ag@PI Aerogel Fabric was conducted to study the integration with ultralight weight and high conductivity [123]. This fabric combines ultralight weight (0.11 g/cm³) with high conductivity (278.0 S/m), achieving a high SE of 89.4 dB in the X-band and a normalized SSE of 812.7 dB·cm³/g (Figure **6**). Its porous structure synergizes with the silver layer to promote multiple reflections and loss of electromagnetic waves, it exhibits an absorption-dominated shielding mechanism. In the Ag@PI-20 sample (with an $AgNO_3$ concentration of 20%), the absorption loss (SE_A) reaches as high as 69.4 dB, while the reflection loss (SE_R) is only 12.5 dB, with the absorption contribution accounting for approximately 77.6%. The fabric also demonstrates excellent flexibility (>70% performance retention after 200 bends), as well as hydrophobicity and washability, making it an ideal choice for lightweight, flexible electromagnetic protection.

Hierarchically Structured PI/CNT Aerogel was developed for EMI shielding in next-generation electronics, featuring good mechanical adaptability and thermal stability [124]. Its unique "macro-micro-nano" three-level architecture achieves an SE of 71 dB in the X-band and an exceptionally high SSE of 6470 dB·cm²/g. This material exhibits a typical absorption-dominated shielding mechanism, where the absorption loss consistently exceeds the reflection loss. The interpenetrating CNT network provides efficient charge transport pathways, resulting in significant ohmic loss. Furthermore, the numerous heterogeneous

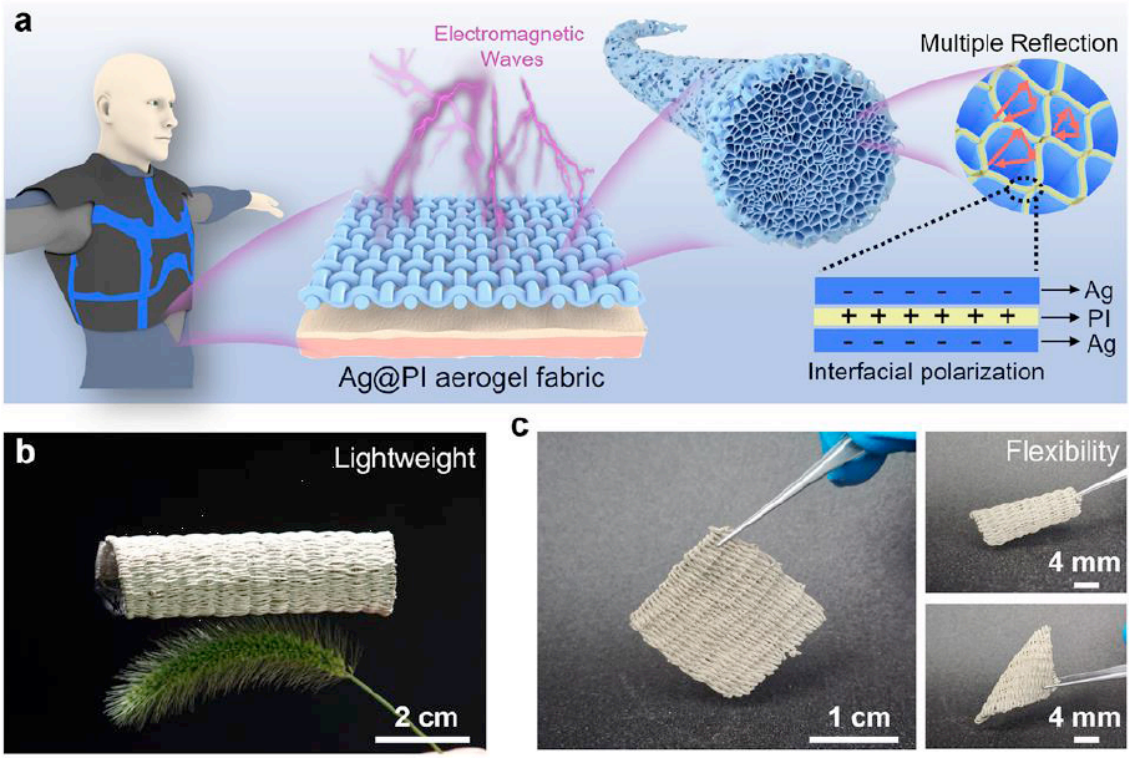

Figure 6: (**a**) Schematic of the electromagnetic interference shielding mechanism of the Ag@PI aerogel fabric. (**b–c**) Photograph of Ag@PI aerogel fabric. Reproduce with permission [123] Copyright, 2023 Elsevier.

interfaces between the PI matrix and the CNTs induce strong interfacial polarization relaxation. Finally, the omasum-like micro-folds and macro-radial pore channels constitute an extremely tortuous internal path, which enhances multiple internal reflections. The material exhibits a negative Poisson's ratio (approximately -0.28) and excellent mechanical stability, evidenced by a high resilience efficiency of 98.2% retained after 500 cycles. At a CNT loading of 67 wt%, a compressive strength of 82.0 kPa is achieved with a total precursor concentration (PAA + CNT) of 50 wt%.

3.5. Silicon Rubber

Compared to other organic polymers, silicones possess unique physicochemical characteristics such as high elasticity, flexibility, and aging resistance. They also offer diversity in base polymer form (solid, liquid, and gel), curing temperature (high temperature, room temperature), curing mechanism (addition, condensation, free radical), and molding processes [125-130]. This grants silicone rubber-based composites a high degree of designability, allowing the selection of the base polymer form, curing temperature, and curing method according to specific application scenarios. Properties like hardness, flexibility, elasticity, stretchability, and mechanical performance can be adjusted over a wide range to meet the diverse needs of practical industrial applications. Over the past decade, high-performance silicone rubber-based EMI composites have been widely researched and applied due to these advantages.

Nickel-Plated Carbon Fiber/Silicone Rubber Composite was developed as an aircraft EMI shielding coating with flame retardancy and Joule heating capability [131]. As the filler (Ni@CF) loading increased from 20 to 60 wt%, the surface sheet resistance of the composite plummeted from 65.5 to 5.1 Ω/□, indicating a significant enhancement in electrical conductivity. Correspondingly, the total shielding effectiveness (SE_T) in the X-band (8.2-12.4 GHz) improved from 20.1 dB to 42.6 dB, yielding an exceptional SE_T/thickness ratio of 60.9 dB/mm at a minimal thickness of 0.7 mm. The shielding mechanism of this material is typically reflection-dominated. This is primarily attributed to the significant impedance mismatch at the interface between the material (featuring highly conductive nickel layers and carbon fiber networks) and air, leading to strong reflection of incident electromagnetic waves at the surface. It combines excellent flame retardancy (withstanding 1300°C) with stable Joule heating performance, has a mechanical strength of 2.3 MPa, and maintains stable shielding performance after harsh treatments.

Gradient Porous Silicone Rubber Composite Foams Containing Silver-Plated Glass Fibers were developed for electromagnetic protection of wearable flexible electronics, high-power instruments, and 5th-Generation communication products [132]. the composite foam achieved an ultrahigh average total shielding effectiveness (SE_T) of 78.6 dB in the X-band (8.2-12.4 GHz), accompanied by a high absorption coefficient (A) of 0.82. Remarkably, a minimum reflection coefficient (R) of 0.06 was observed at 7.68 GHz, indicating an absorption ratio of up to 94% at this frequency. This exceptional absorption performance originates from the synergy of multiple physical processes: firstly, the surface low-conductivity layer facilitates wave incidence; secondly, the intermediate gradient-distributed MWCNT layers and the Fe_3O_4 layer progressively dissipate energy through interfacial polarization, dielectric loss, and hysteresis loss; finally, the underlying highly conductive Ag@GF network strongly reflects the remaining waves, and the reflected waves interact with subsequent incident waves, causing resonance cancellation at specific frequencies, which significantly reduces overall reflection. These materials are flexible and stable, showing almost no performance attenuation after 1000 bending cycles, making them suitable for electromagnetic protection in wearable electronics and 5G devices.

Sandwich-structured CF@Fe_2O_3/(BN/SR) Composite was developed for thermal management, EMI shielding, and electrical insulation in electronic devices [100]. The material achieves synergistic performance optimization by constructing a conductive/magnetic network with 45.5 wt% CF@Fe_2O_3 in the middle layer and filling the outer layers with 20.6 wt% of aligned BN. This specific spatial distribution and filler loading enable the material to achieve a high total EMI shielding effectiveness (SE) of 37.7 dB in the X-band while maintaining excellent electrical insulation (volume resistivity of 6.2×10^{14} Ω·cm, breakdown strength of 26.8 kV/mm). Furthermore, the highly aligned BN network imparts a high in-plane thermal conductivity of 3.86 W/(m·K) to the material, resulting in a superior cooling effect—5.6°C lower than commercial thermal grease—in CPU simulation tests.

3.6. Thermoplastic Elastomers

As hybrid materials composed of soft elastic phases and hard thermoplastic segments, thermoplastic elastomers (TPEs) combine rubber-like elasticity with thermoplastic processability [133-135]. They also offer advantages such as excellent physical and mechanical properties and light weight. In addition, they show good adhesion compatibility with various thermoplastics and strong resistance to chemical solvents. These characteristics make them ideal choice for multiple

industrial fields [136]. Unlike thermosetting rubbers, TPEs achieve molecular chain connection solely through physical cross-linking. This thermally reversible characteristic grants them the advantage of recyclability.

Polystyrene/Ethylene-Co-Methyl Acrylate (PS/EMA) co-continuous thermoplastic elastomeric blend composites have been developed for efficient microwave shielding and thermal management in next-generation wearable electronics [97]. Through the selective dispersion of functionalized carbon nanomaterials, the material with 15 wt% filler achieves an SE of -34.9 dB to -36.7 dB in X-band and a thermal conductivity of ~0.85 W/m·K, When the filler content exceeds the critical percolation threshold (>3-5 wt%), a dense, interconnected three-dimensional conductive network forms within the EMA phase, causing the shielding mechanism to rapidly shift toward absorption domination. This is primarily due to the network of functionalized carbon nanomaterials with high aspect ratios, which introduces numerous heterogeneous interfaces and defects, enhancing interfacial polarization and dipole polarization. Simultaneously, electromagnetic waves undergo multiple reflections and scattering within the three-dimensional network, with their energy being efficiently dissipated as heat through ohmic losses and dielectric polarization relaxation induced by functional groups (-COOH, -OH).

Low-Density Polyethylene/Ethylene-Octene Copolymer (LDPE/EOC)/Vulcan Carbon Black (VCB) composites are developed for EMI shielding in modern electronic devices, integrating thermal conductivity, electrical conductivity, and mechanical stability [137]. With 30 wt% conductive carbon black, they exhibit an SE of -26 dB in X-band and a thermal conductivity of 0.46 W/m·K, The shielding mechanism is predominantly absorption-driven, which is attributed to the formation of extensive conductive networks that promote ohmic and polarization losses within the bulk material, while the relatively lower surface reflection is mitigated by the impedance matching effect arising from the dispersed conductive filler within the polymer matrix.

Selective Laser Sintering (SLS) 3D-Printed Thermoplastic Polyurethane (TPU) porous composites were developed for piezoresistive sensing and broadband electromagnetic interference shielding [138]. Based on MWCNT/GE hybrid fillers and porous structural design (Figure **7**), the material demonstrates a significant negative piezoresistive effect with a gauge factor of up to -70. Simultaneously, the combination of the 3D conductive network and the multi-scale porous architecture (featuring inherent lattice pores and nano-defects from sintering) enables efficient broadband electromagnetic dissipation. The EMI shielding mechanism is predominantly absorption-based, facilitated by multiple internal reflections and subsequent Ohmic losses within the conductive skeleton. This is quantitatively evidenced by an absorption coefficient of 0.70–0.91 in the Ku-band (12–18 GHz) for a 10.6 mm thick G20 sample, and near-perfect absorption (>0.99) from 300 GHz to 1 THz for a 2 mm thick sample.

3.7. Polyvinyl Alcohol (PVA)

Polyvinyl alcohol is a water-soluble synthetic polymer whose backbone consists solely of carbon atoms, and it is biodegradable under both aerobic and anaerobic conditions [139, 140]. This material possesses multiple characteristics, such as tunable viscosity, film-forming ability, emulsifying properties, dispersing power, tensile strength, and flexibility, along with thermal stability, adhesiveness, and solvent tolerance. Consequently, it is widely used in textile and paper sizing, fiber coatings, adhesives, emulsion polymerization, packaging and agricultural films, and the production of polyvinyl butyral [141,142].

Ag-modified PVA/Fe_2O_3 Composite Nanofibers were developed for EMI shielding, making them suitable for lightweight applications in aircraft, spacecraft, and automobiles [98]. Optimized with a 200 nm Ag layer and 10 wt% Fe_2O_3, the material achieves an SE of 45.2 dB in the X-band, dominated by absorption loss. This absorption-dominant behavior is attributed to the highly porous nanofibrous network, which provides a large specific surface area and

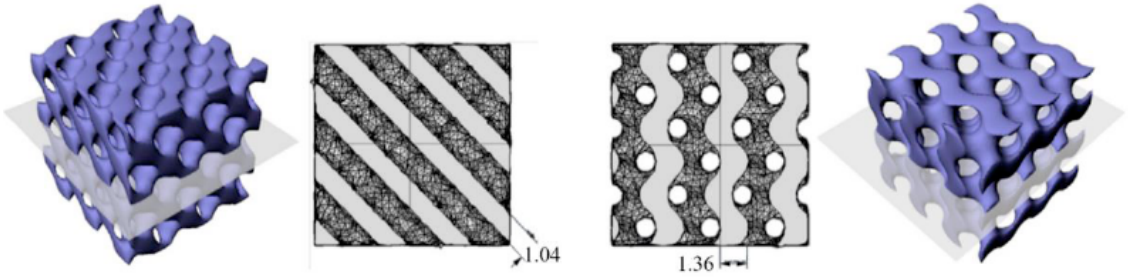

Figure 7: The structure of the material and the cross-sectional area and thickness of the trabeculae. Reproduce with permission[138] Copyright, 2020 MDPI.

facilitates multiple internal reflections and subsequent Ohmic dissipation of EM waves within the material. The conductive Ag layer (with a volume resistivity as low as 6.9×10^{-4} Ω·cm) and the incorporated Fe_2O_3 nanoparticles synergistically enhance dielectric/magnetic losses. The material is suitable for lightweight electromagnetic shielding applications in fields such as aerospace.

PVA/PAA-PEDOT:PSS-TA Composite Hydrogel was developed for human motion sensing, and EMI shielding, making it suitable for flexible wearable devices [143]. This material exhibits excellent mechanical properties (tensile strain up to 640%) and strong adhesion (adhesion strength of 14.97 kPa). Its SE in the X-band reaches 29.51 dB (at 80% water content), The shielding mechanism is overwhelmingly absorption-dominated, which is attributed to the synergistic effects of (1) the conductive PEDOT:PSS network promoting Ohmic losses, (2) the high-water content (~80%) and porous hydrogel structure facilitating multi-scale internal reflections and interfacial polarization, and (3) the strong interaction between water molecules and polymer chains enhancing dielectric loss. It also functions as a highly sensitive strain sensor and can be assembled with PDMS to form a triboelectric nanogenerator, making it suitable for wearable sensing and electromagnetic protection applications.

3.8. Other Polymers

A Soy Protein-Based Conductive Adhesive was developed for plywood to enhance mechanical properties and EMI shielding capability, adapting it to indoor electromagnetic pollution protection scenarios [144]. This adhesive achieves dry/wet shear strengths of 1.97 MPa and 1.16 MPa, respectively, representing a significant improvement over pure soy protein adhesive. Its total EMI SE in the X-band reaches 38.04 dB, with 74% attributed to absorption. This absorption-dominated behavior is attributed to a synergistic physical mechanism: (1) The conductive PANI shell and the PDA-mediated strong interface create extensive interfacial polarization and associated dielectric loss within the nanocomposite; (2) The well-dispersed nanoparticles form a micro-capacitor network, promoting charge accumulation and ohmic loss; (3) The unique multi-layered structure of the plywood, with adhesive layers acting as shielding interlayers, induces multiple internal reflections and scattering of incident electromagnetic waves, significantly prolonging the propagation path and enhancing energy dissipation through absorption, rather than simple reflection.The material also exhibits good flame retardancy, with an increased thermal decomposition temperature of 333.2°C. It features low preparation cost, is environmentally friendly, and aligns well with the requirements of electromagnetic shielding and structural bonding in interior decoration plywood.

MXene@AgNPs-GG/AA Dual-Network Conductive Hydrogel was developed for wearable sensors and EMI shielding, integrating high stretchability, self-adhesion, antibacterial activity, and biocompatibility [145]. The hydrogel demonstrates outstanding comprehensive performance, with a tensile strength of 97 kPa, fracture elongation of 850%, electrical conductivity of 14.04 mS/cm, and an SE of 34.5 dB in the X-band. A detailed deconstruction of the shielding effectiveness reveals an absorption-dominated mechanism. This is attributed to the synergistic effects of (i) conductive loss from the interconnected MXene/AgNPs network, (ii) enhanced interfacial/dipolar polarization at the numerous heterogeneous interfaces (MXene/AgNP/polymer), and (iii) multiple internal reflections within the porous microstructure (pore size ~10 μm), which collectively prolong the propagation path and dissipate incident electromagnetic energy as heat. It also achieves high-sensitivity strain-sensing capability and outstanding antibacterial performance, providing a 100% inhibition rate against *E. coli* and *S. aureus*. These properties make it ideal choice for wearable sensing devices and biocompatible electromagnetic shielding applications.

4. COMMON FILLERS FOR CONDUCTIVE ADHESIVES

4.1. Traditional Metal Fillers

In electromagnetic shielding materials, traditional metal fillers are the most commonly used type in conductive adhesives due to their excellent electrical conductivity and mature processing technology. Depending on the filler material, traditional metal fillers mainly include silver-based, copper-based, and nickel-based systems, among others. Additionally, there are special types such as low-melting-point alloys and composite fillers, each possessing unique performance characteristics and application scenarios [98, 146-151].

Silver-based fillers are the conductive fillers with the excellent performance and the widest application in conductive adhesives. Silver powder has extremely low volume resistivity, providing superior conductive performance, and ranking first among metallic fillers [123, 146, 155, 156]. More importantly, silver exhibits excellent chemical stability, with a slow oxidation rate in air, and even the resulting oxide retains some conductivity. These characteristic allow silver-based conductive adhesives to maintain stable conductive performance under various environmental conditions.

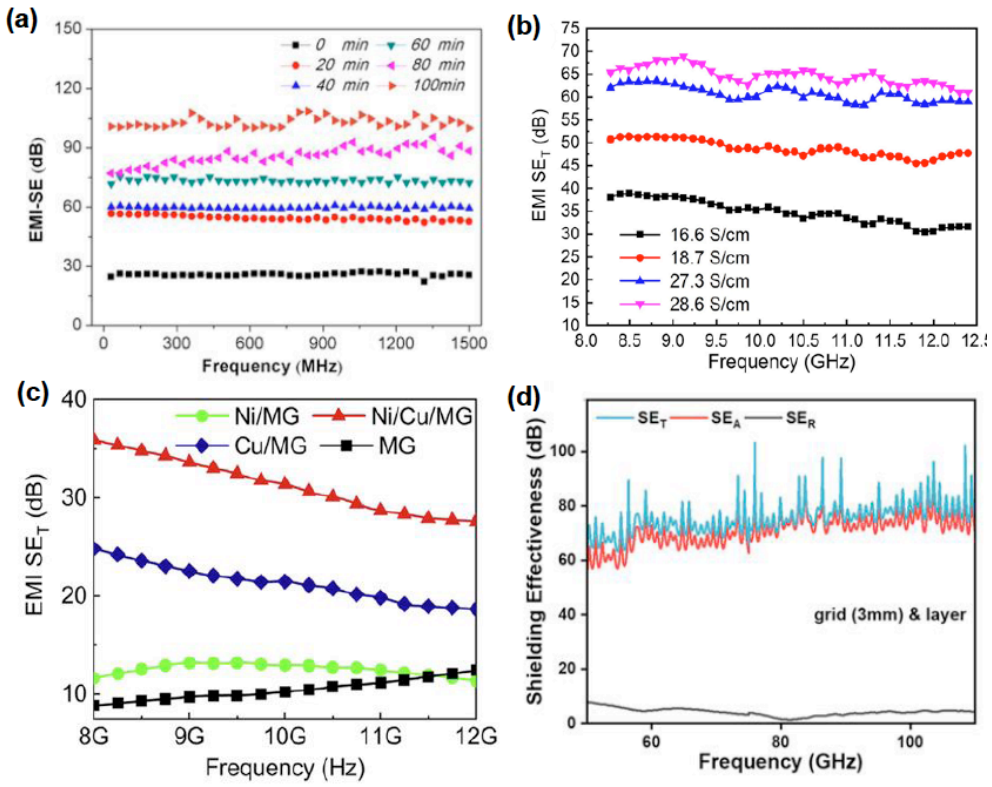

Figure 8: (**a**) EMI-Ses results of CEF-NF/Ag/WPU films, Reproduce with permission[152] Copyright, 2019 Elsevier. (**b**) EMI SE$_T$ of SiO_2@Ag@MF foam as a function of frequency. Reproduce with permission[96] Copyright, 2021 Elsevier. (**c**) EMI SE of MG, Ni/MG, Cu/MG and Ni/Cu/MG. Reproduce with permission[153] Copyright, 2021 Elsevier. (**d**) EMI (SE) and d reflection (SE$_R$) of the 410-μm-thick LMGD with a grid spacing of 3 mm for EMWs at 50–110GHz. Reproduce with permission[154] Copyright, 2020 Springer Nature.

Carbon-Fabric/Ag/Waterborne Polyurethane Composite Film was developed for efficient electromagnetic interference (EMI) shielding in wearable devices and flexible materials, featuring light weight, ultra-thinness, and high reliability [152]. With a thickness of only 0.183 mm, the film achieves a conductivity of 11986.8 S/cm, an SE of 102.9 dB in the X-band (Figure **8a**), and an SSE/t of 5808.7 dB·cm²/g. The shielding mechanism is quantitatively and physically dominated by reflection. Power coefficient analysis reveals a high reflection coefficient (R ≈ 0.845) versus absorption coefficient (A ≈ 0.154). This is due to the excellent conductivity and consequent significant impedance mismatch with air, causing most incident waves to be reflected at the surface by the abundant mobile charge carriers (free electrons) in the continuous Ag network. While the porous structure and internal interfaces contribute to absorption through multiple reflections and ohmic loss (as evidenced by a high potential absorption SE_A of ~78.5 dB), the primary and actual attenuation mechanism remains reflection. Its performance remains stable after ultrasonic treatment, bending cycles, and thermal aging, making it suitable for flexible electronic devices with stringent requirements for thinness and high efficiency.

The SiO_2@Ag@MF Lightweight Superhydrophobic Foam was developed for electromagnetic protection of personal wearable devices, integrating lightweight design, superhydrophobicity, corrosion resistance, and fatigue resistance [96]. This foam has an extremely low density (0.014-0.019 g/cm³), an SE of 65 dB in the X-band (Figure **8b**), and a high SSE/t of 3439 dB·cm³/g, with absorption as the primary mechanism. The fabrication process—based on template-assisted electroless plating and dip-coating—is relatively straightforward and scalable for batch production. The strong covalent Ag-S interface and the robust PDMS/SiO_2 protective layer are key to the material's demonstrated reliability under mechanical bending, compression, and corrosive environments, suggesting good long-term stability for wearable applications. However, the use of silver, a precious metal, raises concerns about material cost and supply chain scalability for mass production.

Although Ag-based conductive adhesives are widely used today, they still face challenges such as electrochemical migration (ECM) and high cost [26, 157-159]. Electrochemical migration is a prominent reliability issue. Under the combined influence of a humid environment and a DC electric field, silver, acting as the anode, ionizes to produce silver ions (Ag^+). These ions migrate toward the cathode under the electric field and are reductively deposited there, forming dendrites. These dendrites can lead to short

circuits between electrodes, causing permanent device failure. This migration tendency of Ag limits its use in applications requiring high reliability, especially in harsh environments.

Besides Ag, other metal fillers have been extensively studied. For example, a Ni/Cu/Amorphous/Cu/Ni Multilayered Magneto-Electric Composite Film was developed for EMI shielding, thermal management, and Joule heating in smart wearable electronics, suitable for ultra-thin and flexible scenarios [153]. With a thickness of only 0.02 mm, the film achieves an SE of 35 dB in the X-band (Figure **8c**) and an exceptionally high SE/thickness ratio of 1750 dB/mm, Quantitative analysis reveals a critical transition from a reflection-dominant to an absorption-dominant shielding mechanism: at 10 GHz, the absorption loss (SE_A) contributes approximately 30 dB, while the reflection loss (SE_R) is only about 5 dB. This excellent absorption-dominated characteristic (SE_A/SE_T > 85%) originates from its unique alternating magneto-electric architecture. The four internally constructed magneto-electrically mismatched interfaces (Ni/Cu and Cu/MG) effectively promote multiple internal reflections of incident electromagnetic waves. Coupled with strong ohmic loss induced by the highly conductive Cu layers, magnetic hysteresis loss from the magnetic Ni and MG layers, and polarization relaxation loss at the abundant heterogeneous interfaces, the electromagnetic energy is efficiently converted and dissipated as heat. dominated by absorption loss. Its tensile strength reaches 1.2 GPa, with no SE decay after 10,000 bending cycles. It also exhibits excellent Joule heating characteristics (heating to 64 °C within 6 s under 0.2 V) and good thermal stability.

Nickel Chain/Acrylic Pressure-Sensitive Adhesive Composite Conductive Adhesive was developed to protect portable electronic products and wearable devices from microwave radiation, realizing tunable EMI shielding[99]. With a thickness of 0.18 mm and 30 wt% filler, the material achieves an SE of 39.97 dB in the X-band, This absorption-dominant characteristic originates from the material's internally unique gradient layered structure (formed via double casting, resulting in an a-PSA-rich layer and a Ni chain-rich layer) and the one-dimensional morphology of the Ni chains. These features synergistically promote multiple internal reflections and scattering of electromagnetic waves, significantly prolonging their propagation path, thereby enhancing energy dissipation in the forms of dielectric loss (primarily from conduction loss and interfacial polarization relaxation) and magnetic loss (arising from the intrinsic magnetism of Ni and eddy current effects). It also possesses excellent adhesion (peel strength 39.56 N/m, shear strength 41.07 kPa) and flexibility, allowing for safe adhesion to various substrates.

In addition to traditional metal fillers, liquid metal (LM) has emerged as a promising candidate material due to its excellent conductivity and intrinsic fluidity[160–163]. Recently, LM has gained prominent value as a frontier material for the development of soft and stretchable EMI shielding materials.

A Liquid metal Eutectic Gallium–Indium (EGaIn) Grid Layer was developed for absorption-dominated and strain-tunable EMI shielding in next-generation wearable and miniaturized soft electronics[154]. This device exhibited absorption-dominated shielding characteristics, with an EMI SE as high as 75 dB in the 50-110 GHz frequency band (Figure **8d**). At the resonant frequency (81.3 GHz), the reflection shielding effectiveness (SE_R) was only 1.4 dB, effectively reducing secondary electromagnetic pollution. The physical origin of this exceptional performance lies in its unique “grid filtering – interlayer multiple internal reflection” mechanism. Incident electromagnetic waves first encounter the top liquid metal grid, whose period matches specific wavelengths, acting as an inductive filter circuit that dissipates part of the energy. The transmitted waves are then strongly reflected by the internal dense liquid metal layer and undergo multiple internal reflections and scattering within the elastomer space between the grid and the metal layer, leading to extensive absorption and conversion into heat, thereby effectively mitigating secondary electromagnetic pollution. Stretchability was excellent, with a maximum elongation of 1223%. The resonant frequency could be tuned from 81.3 GHz to 71.3 GHz at 33% strain, and reached 77 GHz at 10% strain, adapting to the frequency band of autonomous driving ADAS radar. After 100 cycles of 100% strain, the EMI SE remained stable at around 70 dB. Liquid metal/textile composite was developed for EMI shielding in stretchable electronic devices, combining high shielding effectiveness and mechanical durability[164]. This material combines high shielding effectiveness with excellent stretchability. with a thickness of only 0.35 mm, it achieves an X-band EMI SE of 72.6 dB, while maintaining 66.0 dB and 52.4 dB under 30% and 50% strain, respectively. After 5000 stretch-release cycles, the shielding effectiveness retention rates reached 91.7% at 30% strain and 80.3% at 50% strain. The shielding mechanism is absorption-dominated, with the absorption loss contributing 85.4% of the total SE at 10.3 GHz. This is primarily attributed to the porous structure of the textile itself and the three-dimensional conductive network formed by the liquid metal coating, which guides incident electromagnetic waves to undergo multiple internal reflections and scattering,

thereby dissipating energy efficiently rather than reflecting it directly. The LM coating remained firmly bonded to the substrate, with no significant decrease in EMI SE after 10 minutes of ultrasonic treatment and 100 peel tests. In addition, the tensile strength increased by 58.2% compared to pure textile, and the elongation exceeded 230%.

4.2. Carbon-Based Fillers

Carbon materials, such as graphene, carbon black, carbon fiber, and carbon nanotubes, have been widely used for EMI shielding. They are attractive because of their excellent properties, including high electrical conductivity, low weight, good mechanical strength, chemical stability, low cost, biocompatibility, and environmental friendliness [25, 165-167].

XSBL/SA/CNT Emulsion-Based Adhesive was developed for high-performance wood-based plywood used in electronic environments, providing high bonding strength and EMI shielding[95]. With 15 wt% CNT content, the adhesive achieves a dry shear strength of 4.48 MPa and an electrical conductivity of 15.18 S/m. The resulting three-layer plywood exhibits an SE of 32 dB in the X-band (Figure **9a**), with absorption contributing approximately 80%. This is attributed to the multi-layered structure of the plywood and the incorporated CNTs, which create numerous heterogeneous interfaces and defects, promoting interfacial polarization and dipole relaxation. The covalent amide cross-linking network and strong filler-matrix interface contribute to improved long-term reliability and stability. It is formulated to be environmentally friendly, utilizing renewable sodium alginate (SA) as a key component. From a sustainability perspective, the adhesive system presents advantages in terms of reduced reliance on hazardous chemicals like formaldehyde.

Ag@SBS/CB Composite Foam was developed for high-performance EMI shielding with low metal consumption and is suitable for dynamic compression scenarios[168]. With an extremely low silver content (0.63 vol%), this foam achieves a high X-band SE of 81.3 dB (Figure **9b**) at 5 mm thickness and shows no decay in electrical conductivity after 1500 compression-release cycles. This reliability is attributed to the novel silver-embedded structure within the flexible SBS/CB elastomeric framework, where isolated Ag nanoparticles synergize with CB to maintain conductive pathways under intense deformation, unlike fragile continuous metal coatings. Its near-field shielding performance surpasses that of an aluminum plate of the same thickness, and it can conformally adhere to metal components.

Carbon Nanotube/ultrahigh Molecular Weight Polyethylene (CNT/UHMWPE) Nanocomposite have

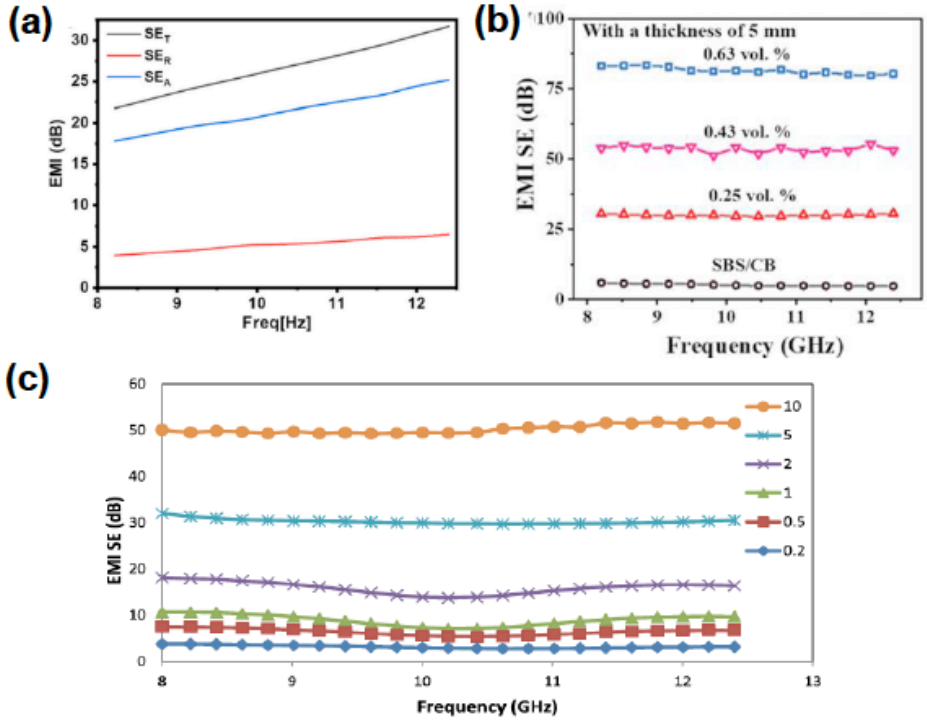

Figure 9: (**a**) Electromagnetic shielding performance test results. Reproduce with permission[95] Copyright, 2025 Elsevier. (**b**) EMI SE of Ag@SBS/CB foam with different silver fractions in X-band. Reproduce with permission[168] Copyright, 2021 Elsevier. (**c**) EMI SE as function of CNT content in the X-band frequency range. Reproduce with permission [169] Copyright, 2015 Elsevier.

been developed for EMI shielding in the electronics industry, fabricated via wet mixing to form a segregated conductive network[169]. This material exhibits an exceptionally low percolation threshold of 0.054 vol%. With 10 wt% CNT content, a 1 mm thick sample achieves an SE of 50 dB in the X-band (Figure **9c**). This structural engineering approach yields an extremely low percolation threshold, which is attributed to the selective localization of carbon nanotubes at the boundaries of UHMWPE powder particles, thereby forming an efficient continuous conductive network and creating a segregated, macroscopic conductive mesh. Furthermore, this unique segregated and relatively thick carbon nanotube layer structure promotes absorption-dominant shielding characteristics. Compared to nanocomposites with finely dispersed carbon nanotubes, this architecture significantly enhances absorption loss while reducing reflection loss.

4.3. MXenes Fillers

MXenes are a class of two-dimensional transition metal carbides and/or nitrides with the general formula Mn+1XnTx (n=1-3) [170]. Layered MXene materials are typically prepared by selectively etching the A layer (which usually contains group IIIA or IVA elements) from the MAX phase precursor (Mn+1AXn). The unique two-dimensional layered structure and abundant surface functional groups endow MXenes with remarkable properties, including high electrical conductivity, surface hydrophilicity, and mechanical stability [171, 172]. MXenes show great potential in the development of EMI shielding materials, as they possess the fundamental characteristics required for constructing efficient EMI shielding macrostructures. These include excellent mechanical properties, outstanding electrical conductivity, large specific surface area and aspect ratio, and exceptional processability in aqueous media.

MXene/Chitosan Composite Film was developed for high-performance EMI shielding with humidity responsiveness, making it ideal for biomass-based flexible electronics[173]. With a thickness of 37 μm and 75% MXene content, the film achieves a conductivity of 1402 S/m and an SE of approximately 34.7 dB in the X-band. At a thickness of 13 μm and 50% MXene content, its specific SE reaches 15,153.9 dB·cm²/g. This absorption dominance is attributed to the well-aligned MXene layers (formed via vacuum-assisted filtration) which create continuous conductive pathways, the intrinsic metallic conductivity of MXene, and the multiple internal reflections of electromagnetic waves within the nacre-like layered structure, effectively dissipating energy. The material also exhibits significant humidity responsiveness, and can sensitively detect changes caused by breathing. The use of chitosan—a biodegradable, non-toxic, and renewable biopolymer—as the matrix significantly enhances the material's green credentials. Combined with good thermal stability and demonstrated biocompatibility, the film aligns with eco-friendly design principles. A critical discussion point is the environmental footprint of MXene synthesis, which involves chemical etching (LiF/HCl). While the end-product is biocompatible, the manufacturing process needs optimization for lower environmental impact.

MXene/ACC Biomimetic Hydrogel was developed for terahertz EMI shielding with strain sensitivity, making it suitable for flexible wearable devices [174]. This hydrogel exhibits absorption-dominated shielding

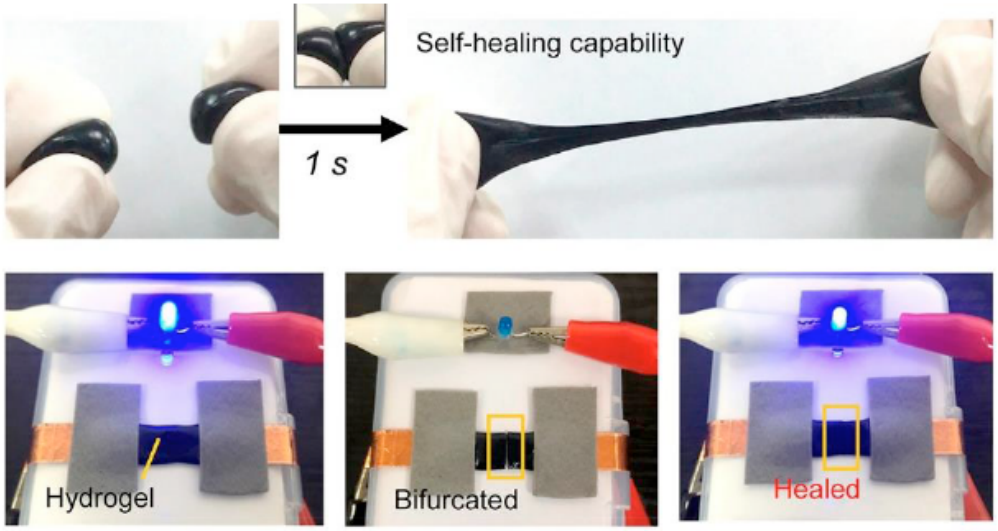

Figure 10: fast self healing capability of the MXene composite hydrogel. Reproduce with permission[174] Copyright, 2021 ACS Nano.

performance in the terahertz band (0.2-2.0 THz), achieving an SE of 45.3 dB at only 0.13 mm thickness. The absorption-dominant mechanism is rigorously attributed to a synergistic physical interplay: the open porous structure promotes multiple internal scattering, extending the propagation path; the interconnected MXene network provides substantial conductive and polarization losses; and the immobilized water-rich environment induces strong dielectric and polarization dissipation, collectively minimizing surface reflection. Its tensile strain exceeds 1500%, and it possesses rapid self-healing capability, instantly recovering its conductivity and shielding performance after cutting and rejoining (Figure **10**). It also functions as a strain sensor for precise monitoring of human activities.

MXene/Aramid Nanofiber Composite Film was developed for efficient EMI shielding and multisource thermal conversion, offering excellent mechanical robustness[175]. Featuring a "brick-and-mortar" structure, a thickness of 7 μm and 80% MXene content, the film achieves an SE of 40.7 dB in the X-band and a specific SE of 22,782.4 dB·cm²/g. It also exhibits outstanding mechanical properties, including a tensile strength of 156.9 MPa, the ability to withstand 4000 cycles of 180° bending, and stability in cryogenic liquid nitrogen environments. Additionally, the film demonstrates multiple thermal management capabilities, such as Joule heating and photothermal conversion.

4.4. Conductive Polymers

Intrinsically conductive polymers (ICPs), such as polypyrrole (PPy) and polyaniline (PANI), offer key advantages including light weight, corrosion resistance, and good flexibility [176, 177]. EMI shielding materials based on ICPs combine corrosion resistance and light weight. These materials exhibit ideal conductivity and excellent performance by absorbing or reflecting electromagnetic radiation over a wide frequency range [178, 179], and they also possess good environmental stability. Widely applicable in electronics, telecommunications, and other fields, they represent an important development direction for EMI shielding materials.

PPy/EVA Hot-Melt Adhesive Composite was developed for EMI shielding in electronic and telecommunication devices, integrating hot-melt adhesive properties and shielding functionality[180]. This material combines the rapid bonding characteristics of hot-melt adhesives with conductive shielding function, exhibiting a low percolation threshold of 0.07. The samples containing 15, 20, and 25 vol% PPy achieve far-field EMI SE values of 22, 27, and 30 dB, respectively, in the 1–300 MHz range, while near-field SE exceeds 80 dB at 1 MHz. The material also shows good environmental stability with no significant decrease in conductivity after 6 months of storage. The hot-melt adhesive format offers excellent manufacturability and scalability via conventional melt-processing techniques (*e.g.*, extrusion), and its inherent adhesive property simplifies assembly by eliminating the need for separate bonding steps in gasket or shield installation, enhancing reliability.

PANI/PVDF Core-Shell Structured Nanofiber Membrane was developed for flexible EMI shielding, making it ideal candidate for wearable electronics and shielding clothing [181]. With a thickness of 1.2 mm, the material achieves an SE of 44.7 dB in the X-band and a specific SE of 372.5 dB/cm, primarily due to the significant impedance mismatch at the core-shell interface which causes strong wave reflection. Concurrently, the hierarchical structure promotes internal multiple reflections and scattering, extending the propagation path and contributing to supplementary absorption. It demonstrates robust mechanical properties, can be folded and bent repeatedly, and shows no significant SE attenuation after 2000 bending cycles. Its surface is superhydrophilic, and its moisture permeability and air permeability far exceed the comfort standards of commercial protective clothing.

Fe_3O_4/C/PPy Core-Shell Composite was developed for EMI shielding, with spin disorder regulating its shielding performance[182]. With a thickness of 0.8 mm, the material achieves an SE exceeding 28 dB in the 1–8.5 GHz frequency band, with absorption loss contributing 88.65%. Efficient electromagnetic wave dissipation is achieved through its multi-interface structures and magneto-electric synergy.

5. CHALLENGES AND PROSPECTS

Current electromagnetic shielding conductive adhesives face multiple key challenges. Achieving high conductivity and shielding performance often requires a high filler loading, which can significantly reduce mechanical properties such as adhesion strength and flexibility. As a result, it is difficult to achieve a synergy between "conductivity-shielding-mechanical" properties. In service environments such as humidity, heat, or thermal cycling, fillers are prone to oxidation, migration, or interfacial bonding failure, causing attenuation of shielding effectiveness. Traditional silver-based fillers also face challenges like electrochemical migration and high cost. While novel low-percolation-threshold fillers like MXene offer excellent performance, their commercialization is still limited by their high costs. Porous materials such as aerogels struggle from weak

mechanical properties. Furthermore, it is challenging to meet the demands for multifunctionality, including thermal conductivity, self-healing, and biocompatibility, under the trend of miniaturization and light-weighting in electronic devices. Future efforts need to focus on achieving high efficiency with low filler loading. Additionally, developing modified MXene or carbon-based composite fillers with high aspect ratios and good compatibility is essential for producing continuous conductive networks under low loadings. Promoting multifunctional integrated design and optimizing hierarchical structures using techniques like directional freezing and 3D printing are crucial steps. Furthermore, upgrading processes such as spraying and *in-situ* polymerization is crucial to enhance the comprehensive performance and application suitability of these materials.

Against the backdrop of rapid electronic device development, electromagnetic interference (EMI) shielding conductive adhesives have become key materials for addressing electromagnetic pollution. Compared to traditional solders and metal shielding materials, they offer significant advantages such as being lead-free and environmentally friendly, low-temperature processable, and compatible with flexible substrates. Their shielding performance is essentially determined by the synergistic effect between the polymer matrix and conductive fillers. Matrices such as epoxy resin, polyurethane, and polyimide provide mechanical adhesion and processability, while fillers including traditional metals, carbon-based materials, MXene, and conductive polymers form efficient conductive networks. Electromagnetic shielding is achieved through reflection, absorption, and multiple-reflection mechanisms governed by percolation theory and quantum tunneling effects. Structural designs such as layered, porous, and honeycomb architectures can significantly enhance material performance. In addition, interfacial modifications like polydopamine (PDA) coating and ligand functionalization further improve conductivity, shielding effectiveness, and mechanical properties. These strategies enable high shielding effectiveness (SE) while maintaining material flexibility and adhesion. Despite significant progress, current conductive adhesives still face numerous challenges. Increasing filler loading to enhance conductivity and shielding performance often degrades mechanical properties. In addition, their long-term stability remains poor under harsh environments such as humidity and thermal cycling.

Existing material systems show a clear deficiency in balancing high-efficiency shielding with multifunctionality—such as thermal conductivity, self-healing, biocompatibility, and environmental responsiveness—amid the trends of miniaturization, lightweighting, and functional integration in electronic devices. To address these challenges, the development of next-generation functional adhesives should focus on the following actionable directions: constructing robust conductive networks at low loadings by developing hybrid fillers with high aspect ratios and good interfacial compatibility (*e.g.*, MXene/CNT, graphene/metal nanowires); enhancing long-term stability in extreme environments through filler surface engineering (*e.g.*, controlled oxide layers, covalent grafting) and interface coupling strategies; employing advanced structural design techniques like directional freezing and 3D printing to fabricate bio-inspired gradient, multilayered, and porous architectures that synergistically optimize impedance matching and attenuation capability, while integrating intelligent responsive features such as self-healing and shape memory; concurrently, promoting the integration of bio-based polymers and renewable fillers, and developing low-energy, low-pollution scalable manufacturing processes to improve environmental friendliness and engineering applicability. With continued innovation in material synthesis, structural optimization, and process upgrades, EMI shielding conductive adhesives are expected to meet the growing demands of high-performance, miniaturized electronic equipment and play an even more crucial role in fields such as flexible electronics, aerospace, and precision instruments.

CONFLICTS OF INTEREST

The author declared no conflicts of interest.

REFERENCES

[1] Saini *et al*. (2012). Microwave Absorption and EMI Shielding Behavior of Nanocomposites Based on Intrinsically Conducting Polymers, Graphene and Carbon Nanotubes, IntechOpen. https://doi.org/10.5772/48779

[2] Wan *et al*. (2017). Graphene paper for exceptional EMI shielding performance using large-sized graphene oxide sheets and doping strategy. Carbon. https://doi.org/10.1016/j.carbon.2017.06.042

[3] Sharma *et al*. (2015). Improved microwave shielding properties of polyaniline grown over three-dimensional hybrid carbon assemblage substrate. Applied Nanoscience. https://doi.org/10.1007/s13204-014-0362-x

[4] Li *et al*. (2024). Flexible regulation engineering of titanium nitride nanofibrous membranes for efficient electromagnetic microwave absorption in wide temperature spectrum. Nano Research. https://doi.org/10.1007/s12274-023-6350-2

[5] Xiao *et al*. (2025). Interfacial Polarization Loss Improvement Induced by the Hollow Engineering of Necklace-like PAN/Carbon Nanofibers for Boosted Microwave Absorption. Advanced Functional Materials. https://doi.org/10.1002/adfm.202316722

[6] Zhang *et al*. (2024). Synchronous deprotonation–protonation for mechanically robust chitin/aramid nanofibers conductive aerogel with excellent pressure sensing, thermal management, and electromagnetic interference shielding. Nano Research. https://doi.org/10.1007/s12274-023-6189-6

[7] Albert *et al*. (2024). Review on recent progress in epoxy-based composite materials for Electromagnetic Interference(EMI) shielding applications. Polymer Composites. https://doi.org/10.1002/pc.27928

[8] Zheng *et al*. (2024). Recent advances in structural design of conductive polymer composites for electromagnetic interference shielding. Polymer Composites. https://doi.org/10.1002/pc.27773

[9] Mo *et al*. (2023). Nanoengineering Natural Leather for Dynamic Thermal Management and Electromagnetic Interference Shielding. Small. https://doi.org/10.1002/smll.202303368

[10] aherian, R. (2016). Experimental and analytical model for the electrical conductivity of polymer-based nanocomposites. Composites Science and Technology. https://doi.org/10.1016/j.compscitech.2015.11.029

[11] Mazaheri, M. *et al*. (2022). Modeling of Effective Electrical Conductivity and Percolation Behavior in Conductive-Polymer Nanocomposites Reinforced with Spherical Carbon Black. Applied Composite Materials. https://doi.org/10.1007/s10443-021-09991-y

[12] Taherian and Reza (2016). Experimental and analytical model for the electrical conductivity of polymer-based nanocomposites. Composites Science and Technology. https://doi.org/10.1016/j.compscitech.2015.11.029

[13] Mazaheri *et al*. (2022). Modeling of Effective Electrical Conductivity and Percolation Behavior in Conductive-Polymer Nanocomposites Reinforced with Spherical Carbon Black. Applied Composite Materials. https://doi.org/10.1007/s10443-021-09991-y

[14] Derakhshankhah, H. *et al*. (2020). Conducting polymer-based electrically conductive adhesive materials: design, fabrication, properties, and applications. Journal of Materials Science: Materials in Electronics. https://doi.org/10.1007/s10854-020-03712-0

[15] Li, Y. and Wong, C.P. (2006). Recent advances of conductive adhesives as a lead-free alternative in electronic packaging: Materials, processing, reliability and applications. Materials Science and Engineering: R: Reports. https://doi.org/10.1016/j.mser.2006.01.001

[16] Wang, D. *et al*. (2013). Dielectric properties of reduced graphene oxide/polypropylene composites with ultralow percolation threshold. Polymer. https://doi.org/10.1016/j.polymer.2013.02.012

[17] Yim, M.J. *et al*. (2008). Review of Recent Advances in Electrically Conductive Adhesive Materials and Technologies in Electronic Packaging. Journal of Adhesion Science and Technology. https://doi.org/10.1163/156856108X320519

[18] Medalia and I., A. (1986). Electrical Conduction in Carbon Black Composites. Rubber Chemistry and Technology. https://doi.org/10.5254/1.3538209

[19] Yim *et al*. (2008). Review of Recent Advances in Electrically Conductive Adhesive Materials and Technologies in Electronic Packaging. Journal of Adhesion Science and Technology. https://doi.org/10.1163/156856108X320519

Xue, Q. (2004). The influence of particle shape and size on electric conductivity of metal–polymer composites. European Polymer Journal. https://doi.org/10.1016/j.eurpolymj.2003.10.011

[20] Miller *et al*. (2005). Polymers in cementitious materials, Rapra Technology.

[21] Tersac and Gilles (2007). Chemistry and technology of polyols for polyurethanes. Milhail Ionescu. Rapra Technology, Shrewsbury, UK. Polymer International.

[22] Jing *et al*. (2005). Electrical conductivity and electromagnetic interference shielding of polyaniline/polyacrylate composite coatings. Journal of Applied Polymer Science. https://doi.org/10.1002/pi.2159

[23] Li *et al*. (2008). Electrical conductivity and electromagnetic interference shielding characteristics of multiwalled carbon nanotube filled polyacrylate composite films. Applied Surface Science. https://doi.org/10.1002/app.22387

[24] Chung and D.D.L (2001). Electromagnetic interference shielding effectiveness of carbon materials. Carbon. https://doi.org/10.1016/j.apsusc.2008.03.077

[25] Sekine *et al*. (9AD). Morphological Behavior of Printed Silver Electrodes with Protective Self-Assembled Monolayers for Electrochemical Migration. ACS Applied Materials & Interfaces. https://doi.org/10.1016/S0008-6223(00)00184-6

[26] Li *et al*. (2023). A survey of conductive and radiated EMI reduction techniques in power electronics converters across wide-bandgap devices. IET Power Electronics.

[27] Jia *et al*. (2022). Evaluation, fabrication and dynamic performance regulation of green EMI-shielding materials with low reflectivity: A review. Composites Part B-Engineering. https://doi.org/10.1049/pel2.12532

[28] Chen *et al*. (2021). Porous aerogel and sponge composites: Assisted by novel nanomaterials for electromagnetic interference shielding. Nano Today. https://doi.org/10.1016/j.compositesb.2022.109652

[29] Januszewski *et al*. (2021). Synthesis and Properties of Epoxy Resin Modified with Novel Reactive Liquid Rubber-Based Systems. Ind. Eng. Chem. Res. https://doi.org/10.1016/j.nantod.2021.101204

[30] Zhang *et al*. (2003). Research on the contact resistance, reliability, and degradation mechanisms of anisotropically conductive film interconnection for flip-chip-on-flex applications. Journal of Electronic Materials. https://doi.org/10.1021/acs.iecr.0c05781

[31] Xiong *et al*. (2025). Nickel conductive adhesive based on bisphenol A epoxy resin modified by CTBN/dicyclopentadiene epoxy resin: Effects of epoxy resin structure on mechanical properties and thermal stability. Journal of Molecular Structure. https://doi.org/10.1007/s11664-003-0214-z

[32] Simon and K. (1988). Hornsäulen-Briquetage von Rüssen, Kr. Borna (mit Tafel 3—4 und sechs Textabbildungen), De Gruyter. https://doi.org/10.1016/j.molstruc.2024.141064

[33] Chen *et al*. (2019). An overview of stretchable strain sensors from conductive polymer nanocomposites. J. Mater. Chem. C. https://doi.org/10.1515/9783112492482-004

[34] Li *et al*. (2012). H_2O_2-Aided Seed-Mediated Synthesis of Silver Nanoplates with Improved Yield and Efficiency. ChemPhysChem. https://doi.org/10.1039/C9TC03655E

[35] Suriati *et al*. (2011). Effects of filler shape and size on the properties of silver filled epoxy composite for electronic applications. Journal of Materials Science: Materials in Electronics. https://doi.org/10.1002/cphc.201101018

[36] Lekawa-Raus *et al*. (2014). Carbon nanotube fiber–silver hybrid electrical conductors. Materials Letters. https://doi.org/10.1007/s10854-010-0082-2

[37] Payandehpeyman, J. *et al*. (2020). Prediction of electrical conductivity of polymer-graphene nanocomposites by developing an analytical model considering interphase, tunneling and geometry effects. Composites Communications. https://doi.org/10.1016/j.matlet.2014.06.177

[38] Wang *et al*. (2013). Dielectric properties of reduced graphene oxide/polypropylene composites with ultralow percolation threshold. Polymer. https://doi.org/10.1016/j.coco.2020.100364

[39] Hashemi, R. and Weng, G.J. (2016). A theoretical treatment of graphene nanocomposites with percolation threshold, tunneling-assisted conductivity and microcapacitor effect in AC and DC electrical settings. Carbon. https://doi.org/10.1016/j.polymer.2013.02.012

[40] Derakhshankhah *et al*. (2020). Conducting polymer-based electrically conductive adhesive materials: design, fabrication, properties, and applications. Journal of Materials Science: Materials in Electronics. https://doi.org/10.1016/j.carbon.2015.09.103

[41] Payandehpeyman *et al*. (2020). Prediction of electrical conductivity of polymer-graphene nanocomposites by developing an analytical model considering interphase, tunneling and geometry effects. Composites Communications. https://doi.org/10.1007/s10854-020-03712-0

[42] Liu and J. (1993). Reliability of Surface-mounted Anisotropically Conductive Adhesive Joints. Circuit World. https://doi.org/10.1016/j.coco.2020.100364

[43] (2004). 2004 Proceedings IEEE/CPMT/SEMI 29th International Electronics Manufacturing Technology Symposium - Copyright. IEEE/CPMT/SEMI 29th International Electronics Manufacturing Technology Symposium (IEEE Cat. No.04CH37585). https://doi.org/10.1108/eb046218

[44] Li, Y. *et al*. (2006). Novel Lead Free Nano-scale Non-Conductive Adhesive (NCA) for Ultra-Fine Pitch Interconnect Applications. 56th Electronic Components and Technology Conference 2006.

[45] Wang, H. *et al*. (2021). Review on Shielding Mechanism and Structural Design of Electromagnetic Interference Shielding Composites. Macromolecular Materials and Engineering.

[46] Lang, L. *et al*. (2024). A review of recent advances in MXenes/polymer-based electromagnetic interference shielding materials. Polymer Composites. https://doi.org/10.1002/mame.202100032

[47] Deng, Y. *et al*. (2024). Transparent electromagnetic interference shielding materials using MXene. Carbon Energy. https://doi.org/10.1002/pc.28627

[48] Tan, S. *et al*. (2025). Achieving Broadband Microwave Shielding, Thermal Management, and Smart Window in Energy-Efficient Buildings. Advanced Functional Materials. https://doi.org/10.1002/cey2.593

[49] Isari, A.A. *et al*. (2024). Structural Design for EMI Shielding: From Underlying Mechanisms to Common Pitfalls. Advanced Materials. https://doi.org/10.1002/adfm.202415921

[50] Srivastava *et al*. (2022). Recent advancements in the electromagnetic interference shielding performance of nanostructured materials and their nanocomposites: a review. J. Mater. Chem. A. https://doi.org/10.1002/adma.202310683

[51] Zecchi *et al*. (2024). A Comprehensive Review of Electromagnetic Interference Shielding Composite Materials. Micromachines. https://doi.org/10.1039/D1TA09522F

[52] Nguyen, Q.-D. and Choi, C.-G. (2024). Recent advances in multifunctional electromagnetic interference shielding materials. Heliyon. https://doi.org/10.3390/mi15020187

[53] González, M. *et al*. Carbon Nanotube Composites as Electromagnetic Shielding Materials in GHz Range. https://doi.org/10.2139/ssrn.4704433

[54] Lin, J. *et al*. (2023). A review on composite strategy of MOF derivatives for improving electromagnetic wave absorption. iScience.

[55] Qiao, J. *et al*. (2024). The vital application of rare earth for future high-performance electromagnetic wave absorption materials: A review. Journal of Materials Science & Technology. https://doi.org/10.1016/j.isci.2023.107132

[56] Wu, Z. *et al*. (2022). Dimensional Design and Core–Shell Engineering of Nanomaterials for Electromagnetic Wave Absorption. Advanced Materials. https://doi.org/10.1016/j.jmst.2023.09.003

[57] Lei *et al*. (2022). Electromagnetic wave absorption superalloy/graphite magnetic nanocapsules applied in wide temperature range. Composites Part B: Engineering. https://doi.org/10.1002/adma.202107538

[58] Wang *et al*. (2018). Carbonized Design of Hierarchical Porous Carbon/Fe_3O_4@Fe Derived from Loofah Sponge to Achieve Tunable High-Performance Microwave Absorption. ACS Sustainable Chem. Eng. https://doi.org/10.1016/j.compositesb.2022.109692

[59] Xiang *et al*. (2023). A simple strategy to develop heterostructured carbon paper/Co nanoparticles composites with lightweight, tunable and broadband microwave absorption. Materials Today Physics. https://doi.org/10.1021/acssuschemeng.8b02089

[60] Wang *et al*. (2021). Flexible and heat-resistant carbon nanotube/graphene/polyimide foam for broadband microwave absorption. Composites Science and Technology. https://doi.org/10.1016/j.mtphys.2023.101030

[61] Wang *et al*. (2021). Polymer-bubbling for one-step synthesis of three-dimensional cobalt/carbon foams against electromagnetic pollution. Journal of Materials Science & Technology. https://doi.org/10.1016/j.compscitech.2021.108848

[62] Wu *et al*. (2020). Optimization, selective and efficient production of CNTs/$Co_xFe_{3-x}O_4$ core/shell nanocomposites as outstanding microwave absorbers. J. Mater. Chem. C. https://doi.org/10.1016/j.jmst.2021.03.048

[63] Li *et al*. (2020). Outstanding comprehensive performance versus facile synthesis: Constructing core and shell-interchangeable nanocomposites as microwave absorber. Journal of Colloid and Interface Science. https://doi.org/10.1039/D0TC01970D

[64] Amikam and Aharoni (1997). Effect of surface anisotropy on the exchange resonance modes. Journal of Applied Physics. https://doi.org/10.1016/j.jcis.2020.01.002

[65] Toneguzzo *et al*. (1997). Observations of exchange resonance modes on submicrometer sized ferromagnetic particles. Journal of Applied Physics. https://doi.org/10.1063/1.364167

[66] Wang *et al*. (2021). Facile synthesis of the three-dimensional flower-like ZnFe2O4@MoS2 composite with heterogeneous interfaces as a high-efficiency absorber. Journal of Colloid and Interface Science. https://doi.org/10.1063/1.364657

[67] Zhou, J. *et al*. (2024). Recent Advances in MXene-Based Aerogels for Electromagnetic Wave Absorption. Small. https://doi.org/10.1016/j.jcis.2020.11.013

[68] Yan, J. *et al*. (2024). Transition metal carbides towards electromagnetic wave absorption application: State of the art and perspectives. Composites Communications. https://doi.org/10.1002/smll.202405968

[69] Capricho *et al*. (2020). Multifunctionality in Epoxy Resins. Polymer Reviews. https://doi.org/10.1016/j.coco.2024.101954

[70] Jin *et al*. (2015). Synthesis and application of epoxy resins: A review. Journal of Industrial and Engineering Chemistry. https://doi.org/10.1080/15583724.2019.1650063

[71] Peng *et al*. (2023). Advances of Modified Lignin as Substitute to Develop Lignin-Based Phenol-Formaldehyde Resin Adhesives. Chemsuschem. https://doi.org/10.1016/j.jiec.2015.03.026

[72] Jiang *et al*. (2024). Bio-based hyperbranched epoxy resins: synthesis and recycling. Chemical Society Reviews. https://doi.org/10.1002/cssc.202300174

[73] Liu *et al*. (2021). Advances in sustainable thermosetting resins: From renewable feedstock to high performance and recyclability. Progress in Polymer Science. https://doi.org/10.1039/D3CS00713H

[74] Zhi *et al*. (2022). A comprehensive review of reactive flame-retardant epoxy resin: fundamentals, recent

developments, and perspectives. Polymer Degradation and Stability. https://doi.org/10.1016/j.progpolymsci.2020.101353

[75] Heintze *et al*. Clinical efficacy of resin-based direct posterior restorations and glass-ionomer restorations – An updated meta-analysis of clinical outcome parameters. Dental Materials. https://doi.org/10.1016/j.polymdegradstab.2022.109976

[76] Dey *et al*. (8AD). Phenolic Resin Derived Hard Carbon Anode for Sodium-Ion Batteries: A Review. ACS ENERGY LETTERS.

[77] May, C. (2018). Epoxy Resins, Routledge.

[78] Hong *et al*. (2012). Selection of thinner for epoxy type resins for neon transformer housing. Journal of Industrial and Engineering Chemistry. https://doi.org/10.1201/9780203756713

[79] Mohammed *et al*. (2012). New class of liquid crystalline epoxy resins: Synthesis and properties. Journal of Industrial and Engineering Chemistry. https://doi.org/10.1016/j.jiec.2012.05.018

[80] Park *et al*. (2004). A study of oxyfluorination of multi-walled carbon nanotubes on mechanical interfacial properties of epoxy matrix nanocomposites. Materials Science and Engineering: A. https://doi.org/10.1016/j.jiec.2011.11.100

[81] Das *et al*. (2013). Biodegradation, cytocompatability and performance studies of vegetable oil based hyperbranched polyurethane modified biocompatible sulfonated epoxy resin/clay nanocomposites. Progress in Organic Coatings. https://doi.org/10.1016/j.porgcoat.2013.03.007

[82] Park *et al*. (2005). Explaining procyclical male–female wage gaps. Economics Letters. https://doi.org/10.1016/j.econlet.2005.01.021

[83] Jeon *et al*. (2013). Corrosion protection by epoxy coating containing multi-walled carbon nanotubes. Journal of Industrial and Engineering Chemistry. https://doi.org/10.1016/j.jiec.2012.10.030

[84] Li *et al*. (2013). Liquid crystalline epoxy resin based on biphenyl mesogen: Thermal characterization. Polymer. https://doi.org/10.1016/j.polymer.2013.03.043

[85] Adin *et al*. (2022). Effect of particles on tensile and bending properties of jute epoxy composites. Materials Testing. https://doi.org/10.1515/mt-2021-2038

[86] Fu *et al*. A Hierarchical Energy Dissipated Structure Enabled Strong, Ultra-Tough, and Sustainable Adhesives. ADVANCED Functional Materials.

[87] Baroncini *et al*. (2016). Recent advances in bio-based epoxy resins and bio-based epoxy curing agents. Journal of Applied Polymer Science. https://doi.org/10.1002/app.44103

[88] Xiang *et al*. (2020). Applications of epoxy materials in pavement engineering. Construction and Building Materials. https://doi.org/10.1016/j.conbuildmat.2019.117529

[89] Gu *et al*. (2016). An overview of multifunctional epoxy nanocomposites. Journal of Materials Chemistry C. https://doi.org/10.1039/C6TC01210H

[90] Joo, K. *et al*. (2018). High Performance Package-Level EMI shielding of Ag Epoxy Composites with Spray method for High Frequency FCBGA package Application. 2018 IEEE 20th Electronics Packaging Technology Conference (EPTC). https://doi.org/10.1109/EPTC.2018.8654311

[91] Kim *et al*. (2024). Polydopamine-coated iron-nickel alloy and epoxy composites for electromagnetic interference shielding. Journal of Applied Polymer Science. https://doi.org/10.1002/app.56187

[92] Song *et al*. (2025). Construction of rGO-MXene@FeNi/epoxy composites with regular honeycomb structures for high-efficiency electromagnetic interference shielding. Journal of Materials Science & Technology. https://doi.org/10.1016/j.jmst.2024.08.022

[93] Wang *et al*. (2019). Fabrication on the annealed Ti3C2Tx MXene/Epoxy nanocomposites for electromagnetic interference shielding application. Composites Part B: Engineering. https://doi.org/10.1016/j.compositesb.2019.04.050

[94] Luo *et al*. (2025). Development and properties of an emulsion-based adhesive with electromagnetic shielding performance and high bonding strength. International Journal of Biological Macromolecules. https://doi.org/10.1016/j.ijbiomac.2025.147921

[95] Li *et al*. (2021). Robust superhydrophobic and porous melamine-formaldehyde based composites for high-performance electromagnetic interference shielding. Colloids and Surfaces A: Physicochemical and Engineering Aspects. https://doi.org/10.1016/j.colsurfa.2021.126742

[96] Ghosh *et al*. (2022). Carbon nanotubes and carbon nanofibers based co-continuous thermoplastic elastomeric blend composites for efficient microwave shielding and thermal management. Composites Part A: Applied Science and Manufacturing. https://doi.org/10.1016/j.compositesa.2022.107118

[97] Kim *et al*. (2012). Fabrication and EMI shielding effectiveness of Ag-decorated highly porous poly(vinyl alcohol)/Fe2O3 nanofibrous composites. Materials Chemistry and Physics. https://doi.org/10.1016/j.matchemphys.2012.06.008

[98] Wang, C. *et al*. (2022). Effective fabrication of flexible nickel chains/acrylate composite pressure-sensitive adhesives with layered structure for tunable electromagnetic interference shielding. Advanced Composites and Hybrid Materials. https://doi.org/10.1007/s42114-022-00482-7

[99] Guo *et al*. (2022). Flexible and insulating silicone rubber composites with sandwich structure for thermal management and electromagnetic interference shielding. Composites Science and Technology. https://doi.org/10.1016/j.compscitech.2021.109253

[100] Zafar *et al*. (2012). Polyurethane: An Introduction, IntechOpen. https://doi.org/10.5772/2416

[101] Asthana *et al*. (1996). Expanded polystyrene composite door shutters —an alternative to wooden door shutters. Construction and Building Materials. https://doi.org/10.1016/0950-0618(95)00094-1

[102] Strobech and Chr. (1990). Polyurethane adhesives. Construction and Building Materials. https://doi.org/10.1016/0950-0618(90)90042-Y

[103] Haber *et al*. (2012). Mechanical and environmental loading of concrete beams strengthened with epoxy and polyurethane matrix carbon fiber laminates. Construction and Building Materials. https://doi.org/10.1016/j.conbuildmat.2011.06.063

[104] Zou *et al*. (2026). Eco-friendly waterborne polyurethane-based coatings with spontaneously formed gradient distribution architectures achieved absorption-enhanced electromagnetic interference shielding and infrared stealth. Composites Part A: Applied Science and Manufacturing. https://doi.org/10.1016/j.compositesa.2025.109297

[105] Wang *et al*. (2020). Self-healing and flexible carbon nanotube/polyurethane composite for efficient electromagnetic interference shielding. Composites Part B: Engineering. https://doi.org/10.1016/j.compositesb.2020.108015

[106] Bai *et al*. (2023). Composite polymeric film for stretchable, self-healing, recyclable EMI shielding and Joule heating. Chemical Engineering Journal. https://doi.org/10.1016/j.cej.2023.147382

[107] Tolvanen *et al*. (2024). Application of Multilayered Blend Films as Soft, Stretchable, Self-Adhesive, and Self-Healing Absorption-Dominant EMI Shielding and Microwave Absorber. Advanced Materials Interfaces. https://doi.org/10.1002/admi.202300960

[108] Olabisi *et al*. (2015). Handbook of Thermoplastics, Plastics Engineering. https://doi.org/10.1201/b19190

[109] Yao *et al*. (2019). Nanocrystalline cellulose/fluorinated polyacrylate latex via RAFT-mediated surfactant-free emulsion polymerization and its application as waterborne textile finishing agent. Journal of Polymer Science Part A: Polymer Chemistry. https://doi.org/10.1002/pola.29390

[110] Bollmann *et al*. (2015). Polyacrylate-water partitioning of biocidal compounds: enhancing the understanding of biocide partitioning between render and water. Chemosphere. https://doi.org/10.1016/j.chemosphere.2014.08.074

[111] Ma *et al*. (2021). Preparation and characterization of polyacrylate composite and its application in superhydrophobic coating based on silicone-modified ZnO. Journal of Coatings Technology and Research. https://doi.org/10.1007/s11998-020-00411-7

[112] Korpusik *et al*. (2023). Degradation of Polyacrylates by One-Pot Sequential Dehydrodecarboxylation and Ozonolysis. J. Am. Chem. Soc. https://doi.org/10.1021/jacs.3c02497

[113] Liang *et al*. (2018). Degradation of Polyacrylate in the Outdoor Agricultural Soil Measured by FTIR-PAS and LIBS. Polymers. https://doi.org/10.3390/polym10121296

[114] Yan *et al*. (2020). Flexible and high-sensitivity piezoresistive sensor based on MXene composite with wrinkle structure. Ceramics International. https://doi.org/10.1016/j.ceramint.2020.06.131

[115] Wang *et al*. (2022). Effective fabrication of flexible nickel chains/acrylate composite pressure-sensitive adhesives with layered structure for tunable electromagnetic interference shielding. Advanced Composites and Hybrid Materials. https://doi.org/10.1007/s42114-022-00482-7

[116] Hong *et al*. (2025). Manufacturing and Characteristic Evaluation of High-Adhesion Acrylic Adhesive Film for Electromagnetic Wave Shielding. Polymers for Advanced Technologies. https://doi.org/10.1002/pat.70290

[117] Kaltenbrunner *et al*. (2013). An ultra-lightweight design for imperceptible plastic electronics. Nature. https://doi.org/10.1038/nature12314

[118] (2018). Polyimides, CRC Press.

[119] Liaw *et al*. (2012). Advanced polyimide materials: Syntheses, physical properties and applications. Progress in Polymer Science. https://doi.org/10.1016/j.progpolymsci.2012.02.005

[120] Iredale *et al*. (2017). Modern advances in bismaleimide resin technology: A 21st century perspective on the chemistry of addition polyimides. Progress in Polymer Science. https://doi.org/10.1016/j.progpolymsci.2016.12.002

[121] Zhuo *et al*. (2023). Anisotropic high-strength polyimide-based electromagnetic interference shielding foam based on cation-π interaction. Chemical Engineering Journal. https://doi.org/10.1016/j.cej.2023.146992

[122] Xue *et al*. (2023). Lightweight and flexible Ag-wrapped polyimide aerogel fabrics for electromagnetic interference shielding. Composites Communications. https://doi.org/10.1016/j.coco.2023.101732

[123] Qiao *et al*. (2025). Bioinspired Polyimide/Carbon Nanotube Aerogels With Core-Radiating and Omasum-Like Morphology toward Excellent Electromagnetic Shielding and Superior Elasticity. Advanced Materials. https://doi.org/10.1002/adma.202513423

[124] Changping, Y. *et al*. (2006). Application of Silicone Rubber in Polymer Based Composites Molding. Materials Review.

[125] Jie, Z. and Shengyu, F. (2002). Progress in Theoretical Research on Conductive Silicone Rubber. Journal of Functional Polymer.

[126] Roy *et al*. (2020). A critical review on the utilization of various reinforcement modifiers in filled rubber composites. Journal of Elastomers and Plastics. https://doi.org/10.1177/0095244319835869

[127] Lai *et al*. (2023). Recent advances for flame retardant rubber composites: Mini-review. Advanced Industrial and Engineering Polymer Research. https://doi.org/10.1016/j.aiepr.2022.12.002

[128] Behera *et al*. (2021). Self-healing elastomers based on conjugated diolefins: a review. Polymer Chemistry. https://doi.org/10.1039/D0PY01458C

[129] Hirai *et al*. (2019). Microstructured rubber and its wettability. Polymer Journal. https://doi.org/10.1038/s41428-019-0192-5

[130] Xu *et al*. (2023). Aircraft coating for electromagnetic interference shielding with flame retardancy and Joule heating capability. Materials Chemistry and Physics. https://doi.org/10.1016/j.matchemphys.2023.127539

[131] Yang *et al*. (2021). Heterogeneous silicon rubber composite foam with gradient porous structure for highly absorbed ultra-efficient electromagnetic interference shielding. Composites Science and Technology. https://doi.org/10.1016/j.compscitech.2021.108663

[132] Banerjee *et al*. (2013). Novel nanostructured polyamide 6/fluoroelastomer thermoplastic elastomeric blends: Influence of interaction and morphology on physical properties. Polymer. https://doi.org/10.1016/j.polymer.2013.10.001

[133] Coran *et al*. (1981). Rubber-Thermoplastic Compositions. Part IV. Thermoplastic Vulcanizates from Various Rubber-Plastic Combinations. Rubber Chemistry and Technology. https://doi.org/10.5254/1.3535842

[134] Banerjee *et al*. (2017). High-Temperature Thermoplastic Elastomers from Rubber–Plastic Blends: A State-of-the-Art Review. Rubber Chemistry and Technology. https://doi.org/10.5254/rct.16.83786

[135] Banerjee *et al*. (2016). An effective strategy to develop nanostructured morphology and enhanced physico-mechanical properties of PP/EPDM thermoplastic elastomers. Journal of Materials Science. https://doi.org/10.1007/s10853-016-9959-7

[136] Paul *et al*. (2025). Selective and Preferential Distribution of Conductive Carbon Filler in Co-Continuous Thermoplastic Elastomeric Blend Composites for Efficient Thermal and Electrical Conductivity With Enhanced Electromagnetic Interference Shielding Effectiveness. Polymer Composites. https://doi.org/10.1002/pc.70508

[137] Rollo *et al*. (2020). On the Synergistic Effect of Multi-Walled Carbon Nanotubes and Graphene Nanoplatelets to Enhance the Functional Properties of SLS 3D-Printed Elastomeric Structures. Polymers. https://doi.org/10.3390/polym12081841

[138] 1 M.L. *et al*. (2012). Enhancement of PVA-Degrading Enzyme Production by the Application of pH Control Strategy. Journal of Microbiology and Biotechnology.

[139] Marušincová *et al*. (2013). Polyvinyl alcohol biodegradation under denitrifying conditions. International Biodeterioration & Biodegradation. https://doi.org/10.1016/j.ibiod.2013.05.023

[140] Shimao and Masayuki (2001). Biodegradation of plastics. Current Opinion in Biotechnology. https://doi.org/10.1016/S0958-1669(00)00206-8

[141] Kawai *et al*. (2009). Biochemistry of microbial polyvinyl alcohol degradation. Applied Microbiology and Biotechnology. https://doi.org/10.1007/s00253-009-2113-6

[142] Zhou *et al*. (2022). A stretchable and adhesive composite hydrogel containing PEDOT:PSS for wide-range and precise motion sensing and electromagnetic interference shielding and as a triboelectric nanogenerator. Mater. Chem. Front. https://doi.org/10.1039/D2QM00690A

[143] Wei *et al*. (2023). A soy protein-based adhesive with improved mechanical and electromagnetic shielding properties by employment of core@double-shell BT@PDA@PANI fillers. Chemical Engineering Journal. https://doi.org/10.1016/j.cej.2023.141512

[144] Pu *et al*. (2025). A highly stretchable, self-adhesive, antimicrobial conductive hydrogel with guar gum/acrylic acid/MXene@AgNPs for multifunctional wearable sensors

and electromagnetic interference shielding. RSC Adv. https://doi.org/10.1039/D5RA00159E

[145] Yan *et al*. (2024). PVDF/Fe_3O_4@pDA@Ag Nanofiber Membranes with Multicore–Shell Structure for EMI Shielding. ACS Applied Polymer Materials. https://doi.org/10.1021/acsapm.4c01543

[146] Yim *et al*. (2016). Electromagnetic interference shielding effectiveness of nickel-plated MWCNTs/high-density polyethylene composites. Composites Part B-Engineering. https://doi.org/10.1016/j.compositesb.2016.04.061

[147] Kim *et al*. (2014). EMI shielding behaviors of Ni-coated MWCNTs-filled epoxy matrix nanocomposites. Surface & Coatings Technology. https://doi.org/10.1016/j.surfcoat.2014.01.030

[148] Hou *et al*. (2020). Excellent Terahertz shielding performance of ultrathin flexible Cu/graphene nanolayered composites with high stability. Journal of Materials Science & Technology. https://doi.org/10.1016/j.jmst.2020.04.007

[149] Lee *et al*. (2017). Density-tunable lightweight polymer composites with dual-functional ability of efficient EMI shielding and heat dissipation. Nanoscale. https://doi.org/10.1039/C7NR02618H

[150] Shen *et al*. (2020). Fabrication of lightweight CMF/RGO/Ag nanocomposite foam via a simple pyrolysis method for highly effective electromagnetic interference (EMI) shielding. 2020 21ST International Conference on Electronic Packaging Technology (ICEPT). https://doi.org/10.1109/ICEPT50128.2020.9202611

[151] Xing *et al*. (2020). Highly flexible and ultra-thin carbon-fabric/Ag/waterborne polyurethane film for ultra-efficient EMI shielding. Materials & Design. https://doi.org/10.1016/j.matdes.2019.108227

[152] Ma *et al*. (2021). Ultrathin, flexible, and high-strength Ni/Cu/metallic glass/Cu/Ni composite with alternate magneto-electric structures for electromagnetic shielding. Journal of Materials Science & Technology. https://doi.org/10.1016/j.jmst.2020.12.012

[153] Wei *et al*. (2024). Liquid Metal Grid Patterned Thin Film Devices Toward Absorption-Dominant and Strain-Tunable Electromagnetic Interference Shielding. Nano-Micro Letters. https://doi.org/10.1007/s40820-024-01457-7

[154] Zhu *et al*. (7AD). PET/Ag NW/PMMA transparent electromagnetic interference shielding films with high stability and flexibility. NANOSCALE.

[155] Zhang *et al*. (2021). Investigation into Electrical Conductivity and Electromagnetic Interference Shielding Performance of Ag/TPU Hybrids Filled with Various Silver Fillers. 2021 5TH IEEE Electron Devices Technology & Manufacturing Conference (EDTM). https://doi.org/10.1109/EDTM50988.2021.9420946

[156] Wu *et al*. (2025). Microstructure/properties and resistance to electrochemical migration of electrodeposited Ag-Sn alloy thin films. Surfaces and InterfaCES. https://doi.org/10.1016/j.surfin.2025.107180

[157] Yang *et al*. (2022). Effect of Ag coating on the oxidation resistance, sintering properties, and migration resistance of Cu particles. journal of alloys and compounds. https://doi.org/10.1016/j.jallcom.2022.166271

[158] Noh *et al*. (2011). Microstructure, Electrical Properties, and Electrochemical Migration of a Directly Printed Ag Pattern. Journal of Electronic Materials. https://doi.org/10.1007/s11664-010-1408-9

[159] Zhang *et al*. (2014). Liquid Metal/Metal Oxide Frameworks. Advanced Functional Materials. https://doi.org/10.1002/adfm.201304064

[160] Haque *et al*. (2024). Electrically Conductive Liquid Metal Composite Adhesives for Reversible Bonding of Soft Electronics. Advanced Functional Materials. https://doi.org/10.1002/adfm.202304101

[161] Bartlett *et al*. (2016). Stretchable, High-k Dielectric Elastomers through Liquid-Metal Inclusions. Advanced Materials. https://doi.org/10.1002/adma.201506243

[162] Tutika *et al*. (2021). Self-healing liquid metal composite for reconfigurable and recyclable soft electronics. Communications Materials. https://doi.org/10.1038/s43246-021-00169-4

[163] Jia *et al*. (2020). Stretchable Liquid Metal-Based Conductive Textile for Electromagnetic Interference Shielding. ACS Appl. Mater. Interfaces. https://doi.org/10.1021/acsami.0c14397

[164] Wang *et al*. (2017). Biomass derived carbon for energy storage devices. J. Mater. Chem. A. https://doi.org/10.1039/C6TA08742F

[165] Das *et al*. (2000). Electromagnetic interference shielding effectiveness of carbon black and carbon fibre filled EVA and NR based composites. Composites Part A: Applied Science and Manufacturing. https://doi.org/10.1016/S1359-835X(00)00064-6

[166] Du *et al*. (2008). Approaching ballistic transport in suspended graphene. Nature Nanotechnology. https://doi.org/10.1038/nnano.2008.199

[167] Shen *et al*. (2021). Robust and flexible silver-embedded elastomeric polymer/carbon black foams with outstanding electromagnetic interference shielding performance. Composites Science and Technology. https://doi.org/10.1016/j.compscitech.2021.108942

[168] Al-Saleh and H., M. (2015). Influence of conductive network structure on the EMI shielding and electrical percolation of carbon nanotube/polymer nanocomposites. Synthetic Metals. https://doi.org/10.1016/j.synthmet.2015.03.032

[169] Yang *et al*. (2022). Biomimetic Porous MXene Sediment-Based Hydrogel for High-Performance and Multifunctional Electromagnetic Interference Shielding. ACS Nano. https://doi.org/10.1021/acsnano.2c06164

[170] Wang *et al*. (2022). Flexible and mechanically strong MXene/FeCo@C decorated carbon cloth: A multifunctional electromagnetic interference shielding material. Composites Science and Technology. https://doi.org/10.1016/j.compscitech.2022.109337

[171] Liu *et al*. (2021). MXene confined in shape-stabilized phase change material combining enhanced electromagnetic interference shielding and thermal management capability. Composites Science and Technology. https://doi.org/10.1016/j.compscitech.2021.108835

[172] Liu *et al*. (2020). Well-aligned MXene/chitosan films with humidity response for high-performance electromagnetic interference shielding. Carbohydrate Polymers. https://doi.org/10.1016/j.carbpol.2020.116467

[173] Zhu, Y. *et al*. (2021). Multifunctional Ti3C2TxMXene Composite Hydrogels with Strain Sensitivity toward Absorption-Dominated Electromagnetic-Interference Shielding. ACS nano. https://doi.org/10.1021/acsnano.0c08830

[174] Liu *et al*. (2024). Ultrafine Aramid Nanofiber-Assisted Large-Area Dense Stacking of MXene Films for Electromagnetic Interference Shielding and Multisource Thermal Conversion. ACS Appl. Mater. Interfaces. https://doi.org/10.1021/acsami.4c09426

[175] Chen *et al*. (2025). The copper sulfide coating on polyacrylonitrile with a chelating agent of ethylenediaminetetraacetic acid by an electroless deposition method and its EMI shielding effectiveness. Journal of Applied Polymer Science.

[176] Song *et al*. Flexible graphene/polymer composite films in sandwich structures for effective electromagnetic interference shielding. CARBON.

[177] Kuang *et al*. Facile preparation of lightweight high-strength biodegradable polymer/multi-walled carbon nanotubes nanocomposite foams for electromagnetic interference shielding. CARBON.

[178] Wang *et al*. (2025). Silver nanoparticles/graphene oxide decorated carbon fiber synergistic reinforcement in epoxy-based composites. POLYMER.

[179] Pomposo *et al*. (1999). Polypyrrole-based conducting hot melt adhesives for EMI shielding applications. Synthetic Metals. https://doi.org/10.1016/S0379-6779(99)00061-2

[180] Chen *et al*. (2025). Flexible and Robust Core–Shell PANI/PVDF@PANI Nanofiber Membrane for High-Performance Electromagnetic Interference Shielding. Nano Letters. https://doi.org/10.1021/acs.nanolett.3c05021

[181] Shukla and Vineeta (2020). Role of spin disorder in magnetic and EMI shielding properties of Fe3O4/C/PPy core/shell composites. Journal of Materials Science. https://doi.org/10.1007/s10853-019-04198-w